JOURNAL OF GEOPHYSICAL RESEARCH, VOL. 96, NO. D2, PAGES 3013–3044, FEBRUARY 20, 1991

A Study of the Sources and Sinks of Methane and Methyl Chloroform Using a Global Three-dimensional Lagrangian Tropospheric Tracer Transport Model

JOHN A. TAYLOR[1]

Cooperative Institute for Research in the Environmental Sciences, University of Colorado, Boulder

G. P. BRASSEUR, P. R. ZIMMERMAN, AND R. J. CICERONE[2]

National Center for Atmospheric Research, Boulder, Colorado

Sources and sinks of methane and methyl chloroform are investigated using a global three-dimensional Lagrangian tropospheric tracer transport model with parameterized hydroxyl and temperature fields. By comparison with methyl chloroform observations a global average tropospheric hydroxyl radical concentration of 6.4×10^5 cm^{-3} was found to be consistent with published methyl chloroform emission data for the year 1980. Published methyl chloroform emissions data for 1981–1984 were found to be inconsistent with the observed methyl chloroform concentration increases. A large decrease in hydroxyl radical concentrations could explain the disagreement between the emission data and atmospheric methyl chloroform concentrations, but this is unlikely. Using the hydroxyl radical field calibrated to the methyl chloroform observations, the globally averaged release of methane and its spatial and temporal distribution were investigated. Two source function models of the spatial and temporal distribution of the flux of methane to the atmosphere were developed. The first model was based on the assumption that methane is emitted as a proportion of net primary productivity (NPP). With the average hydroxyl radical concentration fixed, the methane source term was computed as ~ 623 Tg CH_4, giving an atmospheric lifetime for methane ~8.3 years. The second model identified source regions for methane from rice paddies, wetlands, enteric fermentation, termites, and biomass burning based on high-resolution land use data. This methane source distribution resulted in an estimate of the global total methane source of ~611 Tg CH_4, giving an atmospheric lifetime for methane ~8.5 years. The most significant difference between the two models were predictions of methane fluxes over China and South East Asia, the location of most of the world's rice paddies, indicating that either the assumption that a uniform fraction of NPP is converted to methane is not valid for rice paddies, or that NPP is underestimated for rice paddies, or that present methane emission estimates from rice paddies are too high. Using a recent measurement of the reaction rate of hydroxyl radical and methane by Vaghjiani and Ravishankara (G. L. Vaghjiani and A. R. Ravishankara, Rate coefficient for the reaction of OH and CH_4: Implications to the atmospheric lifetime and budget of methane, submitted to *Nature*, 1990) (hereinafter referred to as Vaghjiani and Ravishankara, 1990) leads to estimates of the global total methane source for SF1 of ~524 Tg CH_4 giving an atmospheric lifetime of ~10.0 years and for SF2 ~514 Tg CH_4 yielding a lifetime of ~10.2 years. These results are provisional pending any revision of the reaction rate for hydroxyl radical and methyl chloroform.

INTRODUCTION

Methane is a key chemical species in the chemistry of both the troposphere and the stratosphere. Recent analysis of air in dated ice cores provides very clear evidence that methane concentrations have been rising rapidly since the industrial revolution [*Craig and Chou*, 1982; *Rasmussen and Khalil*, 1984; *Stauffer et al.*, 1985; *Pearman and Fraser*, 1988]. Atmospheric measurements over the past decade also show a rapid rise in global methane concentrations of about 0.8–1% each year [*Blake and Rowland*, 1988; *Steele et al.*, 1987]. The rise in methane concentration is probably, at least partly, a consequence of human activities.

In the troposphere, methane is present in such abundance and is sufficiently reactive that it plays an important role in determining the hydroxyl radical concentration. One- and two-dimensional model studies have indicated that increasing methane concentrations may lead to a substantial decrease in tropospheric hydroxyl radical concentrations [*Isaksen and Hov*, 1987; *Thompson and Cicerone*, 1986]. As the hydroxyl radical is involved in the chemistry of most atmospheric trace gases, releases of methane to the atmosphere will significantly affect the concentration of many trace species including CH_3Cl, CH_3Br, CH_2F_2, $CHClF_2$, CH_2Cl_2, CH_3CCl_3, O_3, and SO_2 [*Ramanathan et al.*, 1987]. Methane is also a major contributor to the greenhouse warming anticipated to occur over the next century [*Dickinson and Cicerone*, 1986].

This paper investigates the magnitude and spatial distribution of methane sources and sinks. The fluxes of methane to the atmosphere are currently the subject of much study using a wide range of approaches. *Cicerone and Oremland* [1988] have reviewed the various estimates of methane sources and sinks. Unfortunately, no one

[1] Also at National Center for Atmospheric Research, Boulder, Colorado.

[2] Now at Department of Geosciences, University of California, Irvine, California.

Paper number 90JD02016.
0148-0227/91/90JD-2016 $05.00

method has yielded definitive answers concerning the sources and sinks of methane. In this study we apply a three-dimensional Lagrangian atmospheric transport model with simple chemistry that allows for the chemical destruction of source gases to examine two possible source functions for the release of methane to the atmosphere. An advantage of this approach to the study of methane is that we include the three-dimensional transport between sources and sinks [*Golombek and Prinn,* 1986].

An important constraint to determining the magnitude of the sources of methane is the hydroxyl radical concentration. The average hydroxyl radical concentration has itself been the subject of much theoretical study and limited direct atmospheric measurement. Using published methyl chloroform (1, 1, 1, trichloroethane) emissions and observed concentration data, the average tropospheric OH radical concentration can be calculated assuming that the primary sink for methyl chloroform is reaction with the hydroxyl radical.

While we have considerable and convincing evidence that atmospheric methane concentrations are rising globally at a rapid rate since the Industrial Revolution, the causes of this rapid rise have been difficult to determine although several are associated with the activities of man [*Cicerone and Oremland,* 1988]. The primary difficulty in determining the cause of the rapid rise in methane is that some 70 to 90% [*Cicerone and Oremland,* 1988] of the methane released to the atmosphere is biogenic in origin. These biogenic sources are highly variable diurnally, seasonally, and spatially. Limited sampling, while producing critical information on methane fluxes, provides very uncertain extrapolations of global estimates of emissions of methane to the atmosphere.

Not only must we estimate the current emissions of methane from biogenic sources, but if we are to determine whether the cause of the atmospheric methane increase, or some component of it, is associated, for example, with biogenic sources, then we must estimate the flux of methane associated with the land cover prior to changes brought about by humans. With the flux of methane computed both prior to and after a change in land use, the net change in the flux of methane to the atmosphere can be computed.

Such information should play an important role in the planning process to mitigate the impacts of the greenhouse warming. For example, replacing dry land with irrigated rice paddy farming would lead to a dramatic change in the flux of methane to the atmosphere, whereas if rice paddies replace wetlands, such as swamps, then only a small change in methane flux to the atmosphere may occur. Scenarios for changes in the methane flux from other biogenic sources can be readily constructed. Of course, such changes in land use and methane flux should be viewed in context with their interaction with the atmospheric sink for methane. To estimate methane fluxes both prior to and after anthropogenic changes, we have developed a model for the biogenic release of methane to the atmosphere based upon a model for net primary productivity (NPP). In this paper we report the results of comparing the NPP-based methane flux estimates with available present day atmospheric methane concentrations. In a following paper the NPP methane flux model will be used to investigate pre-industrial methane concentrations.

ATMOSPHERIC TRACER TRANSPORT MODE

The model used in this study is based upon the Lagrangian tracer modeling approach of *Taylor* [1989]. This modeling approach was adopted because a range of perceived advantages including that by definition the mass of tracer is conserved; the relative simplicity compared with the three-dimensional eddy diffusion approach; the elimination of unwanted numerical diffusion and negative tracer concentrations associated with Eulerian approaches; the ability to advect multiple trace species simultaneously; the ability to easily track the trajectories of releases of chemical species over short time periods within the model; the ability to compare the variation in concentration associated with the model wind field with the observed variability, and the low computational cost: see also discussion of *Walton et al.* [1988].

While we consider the Lagrangian modeling approach to have the above advantages, it should be noted that a large number of air parcels are required to represent model transport on a model grid of fine resolution and to ensure that the fluxes of trace gases between the atmosphere and the sources and sinks are properly represented within the model. Also, the determination of trajectories of real air parcels becomes more uncertain with time. The trajectories computed by the model, using a time step of 24 hours, represent the mean circulation and variation about that mean. An individual trajectory is one possible realization of an air parcel trajectory rather than a purely deterministic air parcel trajectory representing a transport event occurring at a particular time. No modeling approach can be expected to predict the real evolution of tracer concentration over long-time integrations unless all errors in the source distributions, advection, and diffusion are exactly equal to zero. Even the smallest uncertainty in tracer advection within the closed system of a global atmospheric tracer transport model will propagate with each time step until the cumulative uncertainty far outweighs the small uncertainty associated with the individual time step. If the uncertainties in the advection scheme also lead to uncertainties in the total mass of tracer in the model, then uncertainties in the tracer distribution will accumulate more rapidly still.

The above arguments ignore the uncertainties associated with the wind fields used as input to the tracer transport model. Even a perfect tracer transport scheme would only provide a representation of tracer transport consistent with the input wind fields. The more deterministic approaches to tracer transport, such as those developed by *Williamson and Rasch* [1989], are best reserved for the transport of short-lived trace species with concentrations varying rapidly over distances approaching the model resolution. Such schemes would also be important where we wished to forecast tracer concentrations into the short-term future ($\sim$ 10 days) (given accurate initial conditions); however, the Lagrangian scheme would be able to forecast the likely variability in the resulting trajectories.

The modeling approach adopted here uses a stochastic Lagrangian advection scheme to move air parcels representing a known mass of a tracer gas in air according to a wind field on a $2.5° \times 2.5°$ grid with seven vertical levels at 1000, 850, 700, 500, 300, 200, and 100 hPa. The wind field includes a mean and time-varying component.

The availability of good estimates of observed global wind fields at a fine resolution (2.5° × 2.5°) at a number of pressure levels was preferred to using General Circulation Model (GCM) wind fields. However, GCM wind fields could readily be substituted if desired. The mean vertical motion is included within the European Centre for Medium Range Weather Forecasting (ECMWF) data set. A component of the rapid vertical transport associated with convective cloud transport is embodied included in this data set. Mixing processes are also modeled through inclusion of a random component in the computation of each air parcel velocity.

The model takes advantage of modern computer architectures, particularly array processing. For example, model simulations with methyl chloroform and methane of 1 year in duration with 100,000 air parcels on the CRAY X-MP/48 at the National Center for Atmospheric Research require only ~ 140–180 s of central processing time for completion. The location of air parcels at each time step may also be stored if so desired to avoid the recalculation of the transport component during subsequent model runs. This approach will be used in future studies involving more complete atmospheric chemistry models which will require short model time steps in order to properly model the spatial and temporal concentration distribution of short-lived chemical species.

The location L, of particle p, in a grid cell located at latitude i, longitude j, level l, and at time t is evaluated as

$$L^P_{ijlt} = L^P_{ijlt-1} + D^P_{ijlt} \quad (1)$$

where D^P_{ijlt} is the displacement of the parcel occurring over one time step and is calculated for each wind speed component u, v, and w independently according to

$$D^P_{ijlt} = \Delta t \left(\bar{r}_{ijl} + \bar{s}_{ijl} N(0,1)\right) \quad (2)$$

where Δt is the time step in seconds, $\bar{r}_{ijl}$ is the appropriate bimonthly time period mean wind velocity (m s^{-1} for displacements in latitude and longitude and hPa s^{-1} in the vertical), and $\bar{s}_{ijl}$ the standard deviation of wind velocity over a bimonthly time period derived at each grid point, and $N(0,1)$ represents a random sample from the standard normal distribution. We transform the Cartesian coordinate displacements to spherical coordinates in the usual way [*Hsu*, 1980], as follows:

$$\lambda^P_{ijlt+1} = \lambda^P_{ijlt} + \frac{u^P_{ijlt}}{aCos\varphi^P_{ijlt}} \quad (3)$$

$$\varphi^P_{ijlt+1} = \varphi^P_{ijlt} + \frac{v^P_{ijlt}}{a} \quad (4)$$

$$Z^P_{ijlt+1} = Z^P_{ijlt} + w^P_{ijlt} \quad (5)$$

where λ^P_{ijlt}, φ^P_{ijlt}, and Z^P_{ijlt} designate the longitudinal, latitudinal, and vertical positions of the air parcel at time t and a is approximated by the Earth's radius.

Equation (3) illustrates a common problem associated with the mathematical representation of the transport of trace species on the sphere, particularly when applying a finite difference approach to a model transport. As we approach the poles, the constant longitudinal grid size in degrees produces a dramatically shrinking cartesian distance which requires that the model time step be reduced in order to ensure numerical stability (the Courant condition), and in Eulerian and semi-Lagrangian finite difference tracer transport, to ensure conservation of tracer mass. Alternative approaches, such as the spectral transport approach, have also been found to be seriously deficient in advecting concentration fields of such quantities as water vapor as a result of Gibbs phenomena, spectral truncation, and dispersion errors associated with spectral transport [*Williamson and Rasch*, 1989]. *Williamson and Rasch* [1989] also note that computational fixes are required to remove physically unrealistic negative water vapor concentrations, implying a failure to conserve tracer mass, from spectral transport models. In the Lagrangian formulation, as described above, the computation of tracer concentration proceeds independently of the calculation of the transport of the air parcels thereby ensuring the conservation of tracer mass. As the poles are approached lines of longitude become closer, longitude loses meaning, and the Lagrangian trajectories will tend toward reproducing the zonal mean displacements rather than the individual longitudinal grid displacements.

The wind velocities in (2) were obtained by nearest neighbor interpolation. The nearest neighbor interpolation appears initially to be an unsophisticated form of interpolation leading to an inaccurate estimate of the wind speed. However, integrated over time or space, the average velocity of a number of air parcels approaches the expected values. Let us say that $\bar{u}$ represents the average air parcel velocity, we define the spatial average $\overline{u_s}$ and temporal average $\overline{u_t}$ as

$$\overline{u}_s = \frac{1}{n} \sum_{i=1}^{n} u_i^P \quad (6)$$

$$\overline{u}_t = \frac{1}{n_t} \sum_{i=1}^{n_t} u_i^P \quad (7)$$

where u_i^P is one air parcel velocity of n air parcels within a grid space at time t. Then in the limit at as either $n \to \infty$ or $n_t \to \infty$ the average values

$$\lim_{n_t \to \infty} \overline{u_t} \to \lim_{n \to \infty} \overline{u_s} \to \bar{u} \quad (8)$$

will approach the observed interpolated mean value. Any bias associated with more sophisticated interpolation schemes will not be present.

The flux of a trace gas into the atmosphere is computed on the basis of estimates of anthropogenic emissions and the exchanges between the atmosphere, the oceans, and the terrestrial biosphere. The flux of a trace gas is added or removed from air parcels present within the corresponding lowest level grid square of the model. Where an air parcel is not present in the lowest-level Eulerian emission grid square of the model during a time step, the flux not added in that time step is included in the next Lagrangian air parcel to arrive at the grid square. The residual flux was found to remain, at each time step, less than 1% of the total flux.

Mixing ratios were derived by translating the Lagrangian parcel coordinates to Eulerian grid coordinates. The Eulerian grid was based on the wind field grid. The divisions in the vertical were centered about the pressure levels with the boundaries lying at the pressure midpoint between the pressure levels. The concentration of a trace gas within each air parcel was then computed. The concentration on the Eulerian grid was calculated as the average of the Lagrangian air parcel concentrations within each grid box.

For the Lagrangian method to be effective, some form of diffusive mixing between air parcels must be included in the model formulation [*Walton et al.*, 1988]. Without diffusive mixing the distribution of air parcel tracer concentrations would continue to broaden requiring increasing spatial and temporal averaging to obtain accurate estimates of tracer concentration. Diffusive mixing can be considered equivalent to allowing air parcels to interact by exchanging tracer mass or to allowing the boundaries of the air parcels to be slowly redefined [*Walton et al.*, 1988].

Diffusive mixing is incorporated into the model by allowing tracer mass to be exchanged between air parcels. The exchange of tracer mass has been implemented by assigning the mass of tracer equivalent to the average concentration computed on the Eulerian grid to each air parcel within the corresponding grid cell. This implementation of diffusive mixing provides consistent results where the number of air parcels ranges from n = 10,000 to n = 1,000,000 on the basis of model simulations with an F-11 like tracer. Calibration of such an approach to diffusive mixing, other than to the spatial distribution of tracer concentration [*Taylor*, 1989], may be possible by comparing observed and predicted autocovariances of tracer concentration.

Wind field data were obtained from the ECMWF in the form of a 5-year record of local 0h and 12h observational analysis fields reported on a 2.5° × 2.5° grid. These data and the analysis procedures used to generate the data are described in detail by *Lorenc* [1981]. Rather than use the ECMWF data directly within the model we reduced the data to a set of coefficients. In this way the computer model did not spend the majority of its execution time reading the wind field data. On theoretical grounds the components of the wind field should be normally distributed [*Justus*, 1978]. To take into account the nonstationarity in the wind fields due to seasonality, the year was divided into six-bimonthly intervals for which the parameters of the normal distributional model were estimated. It was considered that at least problems of severe nonstationarity could thus be avoided. An approximately sixtyfold reduction in wind field parameters required by the model could be achieved through this data reduction scheme. The primary disadvantage of this approach is that only the mean spatial and temporal autocorrelations are preserved.

In order to verify the Lagrangian model transport of the air parcels we studied the dispersion of an inert tracer (with the release and molecular weight equivalent to that of F-11, 250 × 10^9 g yr^{-1}) distributed spatially according to the fluorocarbon emissions model of *Prather et al.* [1987]. We first verified the conservation of tracer mass by calculating the total mass of tracer in the model at each time step. These data were plotted as a function of model time step. The results of a least squares fit yielded a correlation coefficient of 1 and a slope equal to the specified emission of tracer. Figure 1 shows the monthly average concentration of tracer averaged over all air parcels in the model surface layer (bottom 75 hPa of the atmosphere) for the last month of a 5-year model run initialized with zero tracer concentration. Figure 2 presents the annual average latitudinal gradient averaged over the model surface layer for the final year of the model run.

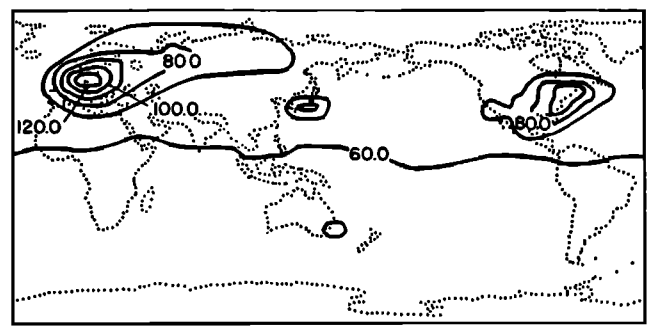

Fig. 1. Monthly average values of mixing ratio (pptv) for an F-11 like tracer calculated in a 5-year model run. Results are for the final month; only surface layer values are shown.

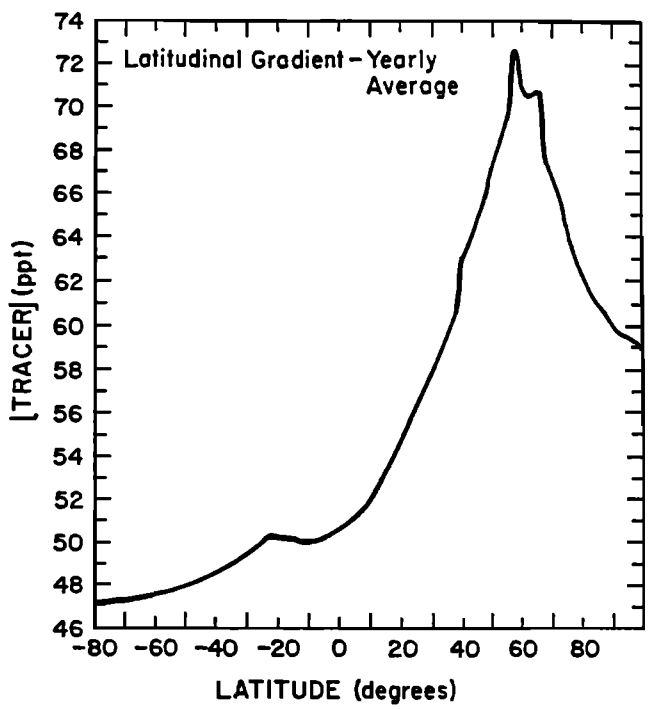

Fig. 2. Annual average of zonal mean calculated for an F-11 like tracer in the fifth year of a 5-year model run. Concentrations are for the model surface layer.

Next using a 5-year model run beginning with zero tracer we computed an estimate of the interhemisphere exchange time τ_{ex} for each month of the year for the duration of the model run according to

$$\tau_{ex} = [C_N - C_S]/\Phi_{N \to S} \quad (9)$$

where C_N is the average northern hemisphere concentration, C_S is the average southern hemisphere concentration, and $\Phi_{N \to S}$ is the flux of tracer from the northern to the southern hemispheres. We obtained a mean value of τ_{ex} of 1.2 years based on the 48-monthly estimates of the last 4 years of the model run. We discarded the first 12 months of the model run to remove the effects of the model initialization on the estimates of τ_{ex}. We also observed a seasonal variation in τ_{ex} with the minimum values of τ_{ex} occurring twice yearly during the northern and southern hemisphere summers and maximum values occuring during spring and autumn. This observation is consistent with the movement of the intertropical convergence zone from one hemisphere to the other. The value of $\tau_{ex} = 1.2$ years obtained in this study compares favorably with the value of 1.1 years derived independently by *Prather et al.* [1987] and *Jacob et al.* [1987]. Note that this value is obtained without introducing an additional diffusion term associated with convective activity in the tropics, as was done for example in the model of *Prather et al.* [1987]. The intensity of interhemispheric exchanges seems therefore to be adequately represented despite the fact that convection is not explicitly simulated. This may be due, in part, to the fact that a substantial fraction of the rapid vertical transport is included in the ECMWF data set.

At the end of the 5-year model run we also computed the number density of air parcels as a function of the 2.5° latitudinal bands. The maximum variation in the number density of air parcels occurs with respect to latitude. Figure 3 shows the theoretical mean number of air parcels, which is just the volume of the latitudinal band divided by the volume of an air parcel, plotted against the number of air parcels actually present within the model 2.5° latitudinal bands at the final model time step of the 5-year model run. Some statistical variation about the theoretical mean number density values is anticipated due to the Monte Carlo component of air parcel velocity computations. Relative to the mean this variation will increase as we approach the poles. Figure 3 shows, even after a 5-year model integration, that the number density of the air parcels is very close that expected.

TROPOSPHERIC HYDROXYL RADICAL FIELD

In view of its central role in atmospheric chemistry, estimating the global tropospheric average hydroxyl radical concentration has been the subject of much study. A number of published estimates of the hydroxyl radical concentration are listed in Table 1. While some estimates of the average hydroxyl radical concentration indicated that a value in the range of 10–100 $\times$ 10^5 molecules cm^{-3} was likely [*Weinstock and Chang,* 1974; *Neely and Plonka,* 1978], more recent results based on the analysis of ^{14}CO data [*Volz et al.,* 1981], and methyl chloroform data [*Prinn et al.,* 1983*a*, 1987] favor a value in the range 3–10 $\times$ 10^5 molecules cm^{-3}.

A number of measurements of the hydroxyl radical concentration have also been obtained [*Perner et al.,* 1987; *Hübler et al.,* 1984; *Platt et al.,* 1988; *Davis et al.,* 1976; *Wang et al.,* 1975]. First attempts at this extremely difficult measurement as summarized in *Hübler et al.* [1984] were an order of magnitude higher than more recent measurements. These first measurements required correction as a result of interference problems and changes in calibration, and they may have been made in polluted, high-oxidant locations.

Summer midday averages of northern mid-latitude measurements, obtained at the Earth's surface, of the hydroxyl radical concentration produced estimates in the range 7–87 $\times$ 10^5 molecules cm^{-3} [*Platt et al.,* 1988; *Perner et al.,* 1987]. These values are in agreement with the average hydroxyl radical concentrations reported in Table 1. The measured midday hydroxyl radical concentrations represent maximum possible hydroxyl radical concentrations which the model predictions of the average hydroxyl radical concentration do not exceed. Model predictions of the two-dimensional hydroxyl radical field [*Brasseur et al.,* 1990; *Volz et al.,* 1981; *Chameides and Tan,* 1981] indicate considerable variability in the global hydroxyl radical field. Rather than compute the full three-dimensional hydroxyl field, which would require a substantial chemical mechanism with concomitant increase in computational requirements, a zonally averaged hydroxyl radical concentration field was computed using the two-dimensional model of *Brasseur et al.* [1990]. In order to reproduce the seasonal variatior in hydroxyl radical concentration, monthly averaged hydroxyl radical fields were calculated. Figure 4 illustrates the resulting hydroxyl radical concentrations (molecules cm^{-3}) for the months January and July. These hydroxyl fields are in good qualitative agreement with those calculated by *Crutzen and Gidel* [1983], *Volz et al.* [1981], and *Allam et al.* [1981]. Ideally, a full three-dimensional hydroxyl radical field would be preferred; however, meridional rather than zonal variations are likely to dominate in the hydroxyl radical field. Hydroxyl radical concentrations in Figure 4 vary from near zero in the polar night to values greater than 10^6 molecules cm^{-3} at midtroposphere over the equator and near the surface at midnorthern latitudes. Until measurements of hydroxyl radical concentrations are obtained routinely and they can be considered to be representative of a large volume of the troposphere, quantitative comparison of model predictions and observations will not be useful. Unfortunately, such measurements are not likely to become available in the near future.

The global mean hydroxyl radical concentration is important in determining the lifetime of many trace species, but the actual spatial distribution of hydroxyl radical in relation to the sources of the trace gases is also critical. For those trace gases that react with OH, lifetimes will be shortest if releases coincide with the highest hydroxyl radical concentrations, such as over the tropics, whereas the opposite is true if trace gas sources are located toward the polar regions where hydroxyl radical concentrations are near zero in winter.

Table 2 lists the mean hydroxyl radical concentrations computed for the globe, northern hemisphere and southern hemisphere for each month of the year. These values were obtained by first using the model of *Brasseur et al.* [1990], which assumed that CO varies with latitude in the two-dimensional model (60 ppb at 90°S, 65 ppb at 45°S, 90 ppb at 0°, 170 ppb at 45°N, 200 ppb at 90°N). Then all the Brasseur et al. OH values were multiplied by a scaling factor determined from methyl chloroform studies described below. Table 2 shows that hydroxyl radical con-

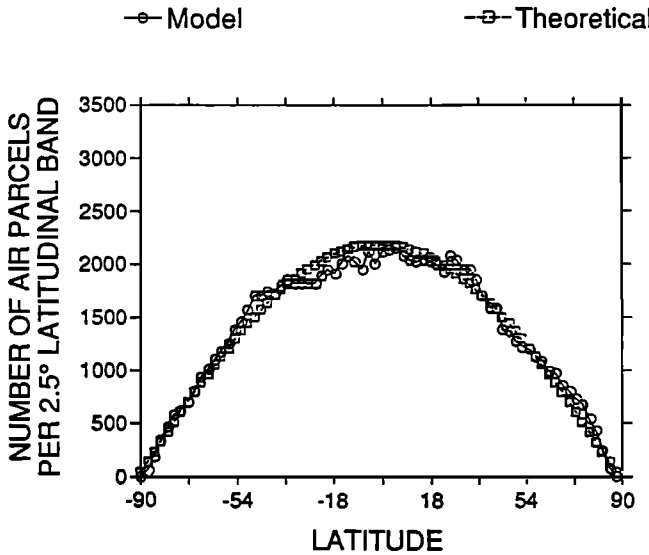

Fig. 3. The average number of air parcels in 2 × 5° model latitudinal bands, as would occur in theory (the volume of the latitudinal band divided by the volume of an air parcel), with the observed number at the end of the 5-year model run.

centrations vary considerably between summer and winter months in the respective hemispheres and that the average hydroxyl radical concentration is higher in the southern hemisphere than the northern hemisphere. This result is consistent with other model studies [*Volz et al.*, 1981].

Methyl Chloroform

It has been recognized for some time that methyl chloroform (CH_3CCl_3) could be used to estimate the average hydroxyl radical concentration [*Lovelock*, 1977; *Singh*, 1977]. Our objective behind modeling methyl chloroform was to deduce the average hydroxyl radical concentration and thus estimate the loss of methane due to reaction with hydroxyl. Methyl chloroform is a solvent which has been increasingly used by industry as a substitute for the more toxic trichloroethylene. Since 1970 annual production and release of methyl chloroform to the atmosphere have more than tripled [*Neely and Plonka*, 1978; *Prinn et al.*, 1987]. As a consequence, concentrations have been observed to be rising rapidly (~ 6% per annum) within the troposphere [*Prinn et al.*, 1987]. This increase in concentration has been the focus of concern in two areas. Once reaching the stratosphere methyl chloroform provides a source of atomic chlorine through photodissociation. Atomic chlorine eventually leads to the the production of "reactive" chlorine (ClO_x) which is thought to be the trace species primarily responsible for the reduction in the ozone layer [e.g., *Anderson et al.*, 1989]. Methyl chloroform is also a greenhouse gas [*Ramanathan et al.*, 1987].

Methyl Chloroform Source Distribution

Methyl chloroform is considered to be entirely anthropogenic in origin. Detailed information concerning the spatial distribution of releases of methyl chloroform to the atmosphere is lacking. In this study we employ the emissions grid originally developed by *Prather et al.* [1987] for the chlorofluorocarbons (CFC), F-11 and F-12. *Prather et al.* [1987] based their emissions grid on electric power consumption because electricity consumption and CFC production are both products generally associated with technologically advanced countries. It was also necessary to divide the world into three economic groupings which related the pattern of CFC use to electricity production. Weighting factors were computed covering the period 1970–1975 and 1976–1982. The validity of the assumption of a relationship between electricity consumption and the release of F-11 and F-12 to the atmosphere was verified by the excellent model predictions of observed F-11 and F-12 atmospheric concentrations [*Prather et al.*, 1987].

TABLE 1. Estimates of the Average Tropospheric Hydroxyl Radical Concentrations Derived From Model Studies

Hydroxyl Radical Concentration, 10^5 molecule cm^{-3}	Source
5–15	*Wofsy et al.* [1972]
50	*Weinstock and Chang* [1974]
7*	*Warneck* [1975]
3.3–5.1	*Singh* [1977]
3	*Crutzen and Fishman* [1977]
4.8 (northern hemisphere)	*Neely and Plonka* [1978]
18.0 (southern hemisphere)	*Neely and Plonka* [1978]
4.5 (6.5) 9.5†	*Volz et al.* [1981]
3.9 (5.3) 6.8†	*Derwent and Eggleton* [1981]
5	*Crutzen and Gidel* [1983]
5 ± 2	*Prinn et al.* [1983a]
7.7 ± 1.4	*Prinn et al.* [1987]

*applies to 30°N latitude

†range with most likely value bracketed

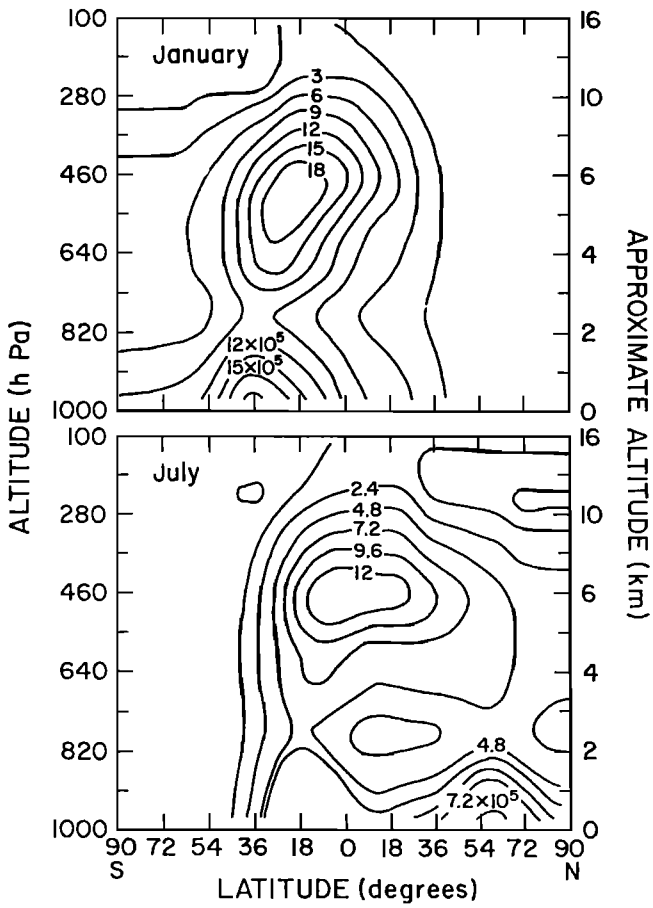

Fig. 4. Monthly averaged two-dimensional hydroxyl radical concentrations computed by *Brasseur et al.* [1990] for the months of January and July.

In this study we employ the same distribution devised by *Prather et al.* [1987] for F-11 and F-12. At each grid square the fraction of the total release of F-11 (or F-12) was computed. The release of methyl chloroform to the atmosphere at each grid square was then computed as the fraction of the total release of methyl chloroform. The F-11, F-12 data of *Prather et al.* [1987], originally developed on an 8° × 10° emission grid, were transformed to the 2.5° × 2.5° model grid.

Golombek and Prinn [1986] developed a 22.5° × 11.5° emission grid for methyl chloroform, F-11 and F-12 based on the data of *Cunnold et al.* [1983*a*, *b*] for F-11 and F-12, and of *Prinn et al.* [1983] for CH_3CCl_3. Their emission grid included overlapping emissions for methyl chloroform and F-11, F-12 exclusively. *Golombek and Prinn* [1986] have indicated that the proportions of the total emissions of F-11 and F-12 to methyl chloroform are not exactly the same. The most significant differences between the proportion of F-11 and F-12 and methyl chloroform occurs in the southern hemisphere. The methyl chloroform emissions in the southern hemisphere are small when compared with the global total methyl chloroform emissions. The temporal changes in observed concentrations of methyl chloroform in the southern hemisphere are dominated by transport of methyl chloroform from the northern hemisphere rather than sources in the southern hemisphere. Should the proportion of annual emissions become available on a finer grid than 22.5° × 11.5°, this would warrant revision of the current spatial distribution of methyl chloroform emissions used in the study reported here.

No data are presently available concerning the seasonal variation in the flux of methyl chloroform to the atmosphere. Observed methyl chloroform concentration data [*Prinn et al.*, 1987] do not indicate the presence of a strong seasonality in emissions. Accordingly, methyl chloroform has been considered to be released at a constant rate throughout the year.

Total annual emissions of methyl chloroform for the period 1979-1984 were those calculated by *Prinn et al.* [1987]. The data reported by *Prinn et al.* [1987] are based on industry estimates of production and sales which are considered accurate to about ±5%. These data have been fitted by *Prinn et al.* [1987] using a simple model which included parameters to take into account the fraction of annual sales that enters the users inventory, the fraction of annual production entering the producers inventory, and the fraction of annual sales to the users that is released to the atmosphere. *Prinn et al.* [1987] computed 2σ uncertainties associated with the emission estimates. Table 3 presents the emission estimates and the calculated range of possible values based on the 2σ uncertainties for the years 1979–1984. These emission estimates should represent the maximum possible emissions to the atmosphere for methyl chloroform because there are no known biospheric sources. However, systematic errors, such as countries not reporting methyl chloroform emissions, as was suggested by *Prinn et al.* [1983] based on the measurements of methyl chloroform by *Rasmussen et al.* [1982] over rural and urban areas in the Peoples Republic of China, would lead to the underprediction of methyl chloroform emissions. Other countries that have not been included in the methyl chloroform production estimates include Eastern Europe and the U.S.S.R. We shall show in this paper that the available atmospheric measurements of methyl chloroform during 1982–1984 are consistent with higher emission rates for methyl chloroform than those reported. Note after completion of this study we became aware of *Midgley*'s [1989] study that reports higher emissions for 1983 and 1984 than *Prinn et al.* [1987].

Methyl Chloroform Model Simulations

Model initialization was performed using a simple latitudinal profile based upon the measured concentrations of methyl chloroform obtained for January 1979 as reported by *Prinn et al.* [1987]. Using the published estimate of methyl chloroform emissions for 1979, the model was initialized with a model run for a 1-year period. Model results are reported on the basis of model runs for the 5-year period 1980–1984.

An average hydroxyl value was selected, and the hydroxyl radical fields of *Brasseur et al.* [1990] scaled to this value. The model was then run forward, including a one year initialization, starting from January 1979. Unfortunately, no one estimate of the hydroxyl radical concentration was able to satisfactorily reproduce the entire series of methyl chloroform observations. A low value for the hydroxyl radical concentration led to the better prediction of methyl chloroform observations during the

TABLE 2. Model Hydroxyl Radical Concentrations for Each Month of the Year

Month	Northern Hemisphere Average	Southern Hemisphere Average	Global Average
1	3.34	10.12	6.73
2	4.14	9.84	6.99
3	5.50	8.36	6.93
4	6.83	6.30	6.56
5	7.18	4.70	5.94
6	7.19	3.83	5.51
7	7.40	3.79	5.59
8	6.95	4.93	5.94
9	5.88	7.07	6.48
10	4.86	8.19	6.52
11	3.89	9.06	6.47
12	3.26	10.26	6.77
Yearly Averages	5.54	7.20	6.37

Hydroxyl radical concentration is 10^5 molecules cm^{-3}.

years 1983–1984 while producing substantial overprediction of methyl chloroform concentrations observed during 1980–1981. A hydroxyl radical concentration consistent with the 1980–1981 years of the methyl chloroform concentration data set resulted in a severe underprediction of the growth in methyl chloroform concentration during 1983–1984.

This inconsistent behavior can be attributed to either a decrease in the average hydroxyl radical concentration with time or to underestimates of the most recent estimates of methyl chloroform emissions. *Prinn et al.* [1987] source strengths show only a small increase over the period while the total atmospheric burden of methyl chloroform increases by 27% with a concomitant increase in bulk loss of methyl chloroform to reaction with the hydroxyl radical. It is this increase in the loss rate which produces the inconsistency with the emission estimates of *Prinn et al.* [1987].

This problem has been investigated in two ways. First, the average hydroxyl radical concentration required to produce the observed increase in methyl chloroform concentration based on the methyl chloroform release estimates of *Prinn et al.* [1987] was computed. These estimates of hydroxyl radical concentration are presented in Figure 5. Figure 5 shows that a decrease in hydroxyl radical concentration of 20% would be required to explain the increase in methyl chloroform concentration for 1984. This result is inconsistent with model predictions of

TABLE 3. Global Emissions of Methyl Chloroform from *Prinn et al.* [1987] and 95% Confidence Range of Possible Values Based on *Prinn et al.* [1987] 2σ Uncertainties

Year	Emission, 10^9g yr^{-1}	95% Confidence Intervals
1979	540.59	515.01–565.87
1980	544.91	519.63–570.19
1981	538.68	513.71–563.65
1982	510.91	487.26–534.56
1983	515.97	492.00–539.94
1984	550.03	512.32–587.74

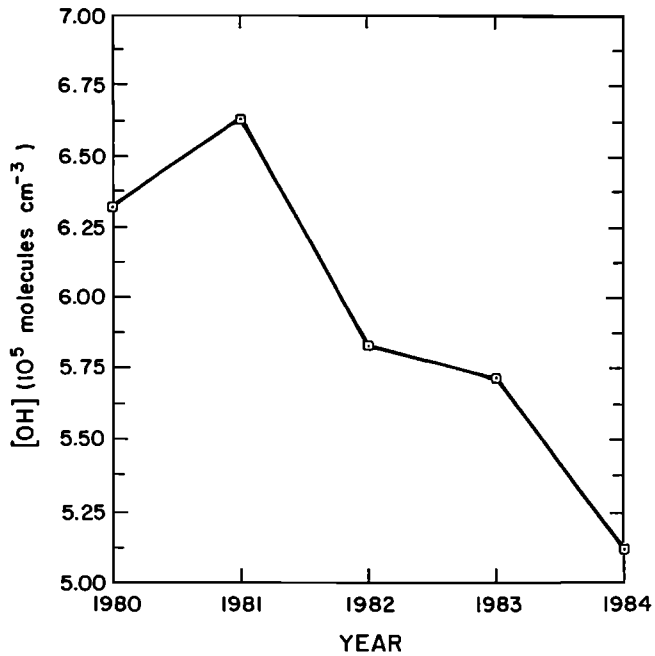

Fig. 5. The calculated global average hydroxyl radical concentration (molecules cm^{-3}) required to produce the observed increase in methyl chloroform concentration based on the methyl chloroform release estimates of *Prinn et al.* [1987]. Such a decrease is judged to be unrealistically large; see text.

the change in tropospheric hydroxyl radical concentration obtained by *Thompson and Cicerone* [1986] and *Isaksen and Hov* [1987]. *Thompson and Cicerone* [1986] estimated that tropospheric hydroxyl radical concentrations would decline by ~ 25–35% over the next 50 years on the basis of various scenarios of future tropospheric trace gas concentrations. *Isaksen and Hov* [1987] assumed that a 1.5% per year increase in tropospheric methane concentration was to occur over the period 1950–2010. This increase in methane concentration was found by *Isaksen and Hov* [1987] to produce a 25% decrease in tropospheric hydroxyl radical concentration. Both studies indicate that ~ 2–2.5% decrease in hydroxyl radical should occur over the 5-year period 1980–1984, an order of magnitude smaller than that required to explain the increase in methyl chloroform concentration based upon the emission estimates of *Prinn et al.* [1987]. It would appear then that the decrease in hydroxyl radical concentration required to explain observed methyl chloroform concentration increases is too large to be realistic. A drop in the hydroxyl radical concentration of the order predicted in Figure 5 over such a short time period would be cause for considerable concern.

A second approach to resolving this inconsistency was to compute the source term required to explain the observed growth in methyl chloroform concentration based on a fixed hydroxyl concentration. Table 4 lists the observed growth in methyl chloroform concentration, the amount lost to reaction with the hydroxyl radical and the required methyl chloroform source estimates based on an average hydroxyl radical concentration of 6.37×10^5 cm^3 which is the average tropospheric hydroxyl radical concentration calculated using the 1980 methyl chloroform emissions and growth rate. This value is consistent with other estimates of the hydroxyl radical concentration as listed in Table 1. The emission values of Table 4 either fall within or just outside the range of possible values suggested by *Prinn et al.* [1987]. The 1981–1984 total emissions of Table 4, 2273×10^9g, is only about 3% higher than the corresponding figure of $2204\text{-}10^9$g derived by *Midgley* [1990]. It should be noted that the calibration of the average hydroxyl radical concentration was based on the methyl chloroform emissions, and the global increase in methyl chloroform concentration for 1980 as the 1980 estimate of methyl chloroform emissions has been the subject of more study [*Prinn et al.*, 1983*a*, 1987] and as the recent methyl chloroform emissions are much more likely to be underestimated because of recent releases in developing countries. Calibration of the average hydroxyl concentration to the 1985 methyl chloroform emissions data of *Prinn et al.* [1987] would require that earlier methyl chloroform emission estimates be revised downward.

Loss to the stratosphere has been implemented on the basis of a simple linear model with no flux occurring at the poles and a maximum loss at the equator. A constant flux to the stratosphere was estimated on the basis of the two-dimensional model of *Brasseur et al.* [1990]. However, the assumption of a constant flux to the stratosphere is not likely to be valid for methyl chloroform because of the changing total methyl chloroform concentration. The planned addition of a stratospheric transport model will allow this exchange to be modeled explicitly. This may lead to the revision downward of the estimated required source of methyl chloroform emissions as reported in Table 4, with the maximum correction possible being $\sim 11 \times 10^9$ g for the 1984 methyl chloroform emissions.

Figure 6 shows the methyl chloroform concentration, computed using the revised methyl chloroform emissions estimates for 1981–1984, as listed in Table 4, at the model surface layer, the bottom 75 hPa (~ 0.75 km) of the atmosphere, for the month of January 1984. Source regions over Europe and North America, South Africa, Japan, and Australia are clearly indicated. Southern Hemisphere oceans are predicted to have a relatively uniform methyl chloroform concentration. The general eastward flow of the atmosphere transports methyl chloroform released over Europe to Eastern Europe and Asia and methyl chloroform from Northeast of the United States to the Atlantic and to Europe.

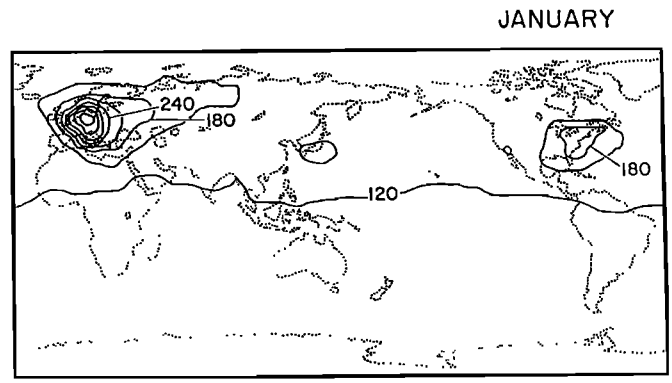

Fig. 6. The methyl chloroform concentration (ppt) computed for the model surface layer for the month of January 1984.

TABLE 4. Methyl Chlorform Sources Required to Explain the Observed Increase in Atmospheric Concentration

Year	Average Concentration,* ppt	Observed Increase, ppt	Observed Increase, g × 10^9	Loss to Stratosphere, g × 10^9	Reaction With Hydroxyl, g × 10^9	Required Source, g × 10^9
1980	100.0	7.56	160.95	40.	343.96	544.91
1981	107.56	5.19	110.50	40.	372.79	523.29
1982	112.75	5.30	112.84	40.	392.72	545.56
1983	118.05	5.15	109.64	40.	412.49	562.13
1984	123.20	7.55	160.74	40.	441.47	642.21
1985	130.75	...	...	...	...	...

*Average of January concentrations at four sites not including Ireland as reported by *Prinn et al.* [1987].

Figure 7 shows the model predictions of methyl chloroform concentration along with the methyl chloroform observations obtained at four Atmospheric Lifetime Experiment/Global Atmospheric Gases Experiment network sites namely Adrigole (Ireland), Cape Meares (Oregon), Ragged Point (Barbados), and Cape Grim (Australia) for the period 1980-1984 as reported by Prinn et al. [1987]. It should be noted that the methyl chloroform concentration measurements reported by *Prinn et al.* [1983*a*, 1987] have been subject to data selection procedures aimed at determining long-term trends. Accordingly, *Prinn et al.* [1983*a*, 1987] have sought to remove high-frequency variation in the methyl chloroform record obtained at these monitoring sites. This high-frequency variation is attributed to "local" pollution. This makes the direct comparison of any model predictions with observations problematic as model predictions include all model events whereas reported measurements do not. Measurements are also collected at coastal sites with the objective of sampling marine air. Measurements are made at particular times of the day and under particular meteorological conditions. Measurements may also be missing as a result of instrumental or other problems. These factors bias reported concentration measurements [*Prinn et al.*, 1983*b*]. However, it is clear that this data selection procedure is warranted when the determination of long-term trends is the goal of the measurement program. Also, data selection is required to remove the effects of local air pollution emanating from sources within a few kilometers of the measurement station.

The methyl chloroform measurements at Adrigole, Ireland, are probably the most strongly affected by local air pollution of the five ALE sites [*Prinn et al.*, 1983*a*, *b*]. Air masses passing over Europe and the United Kingdom were considered to be the cause of the local air pollution [*Prinn et al.*, 1983*a*, *b*]. Some 30% of all observations were removed [*Prinn et al.*, 1983*b*] from the reported monthly mean values for Adrigole [*Prinn et al.*, 1987]. *Prather* [1985] independently confirmed that $\sim$ 30% of all measurements at Adrigole were polluted from sources in Europe.

It is not surprising then that model predictions show far greater variability than the monthly mean methyl chloroform values reported by *Prinn et al.* [1987] as evidenced in Figure 7. However, the agreement between model predictions and observations improve if we compare model

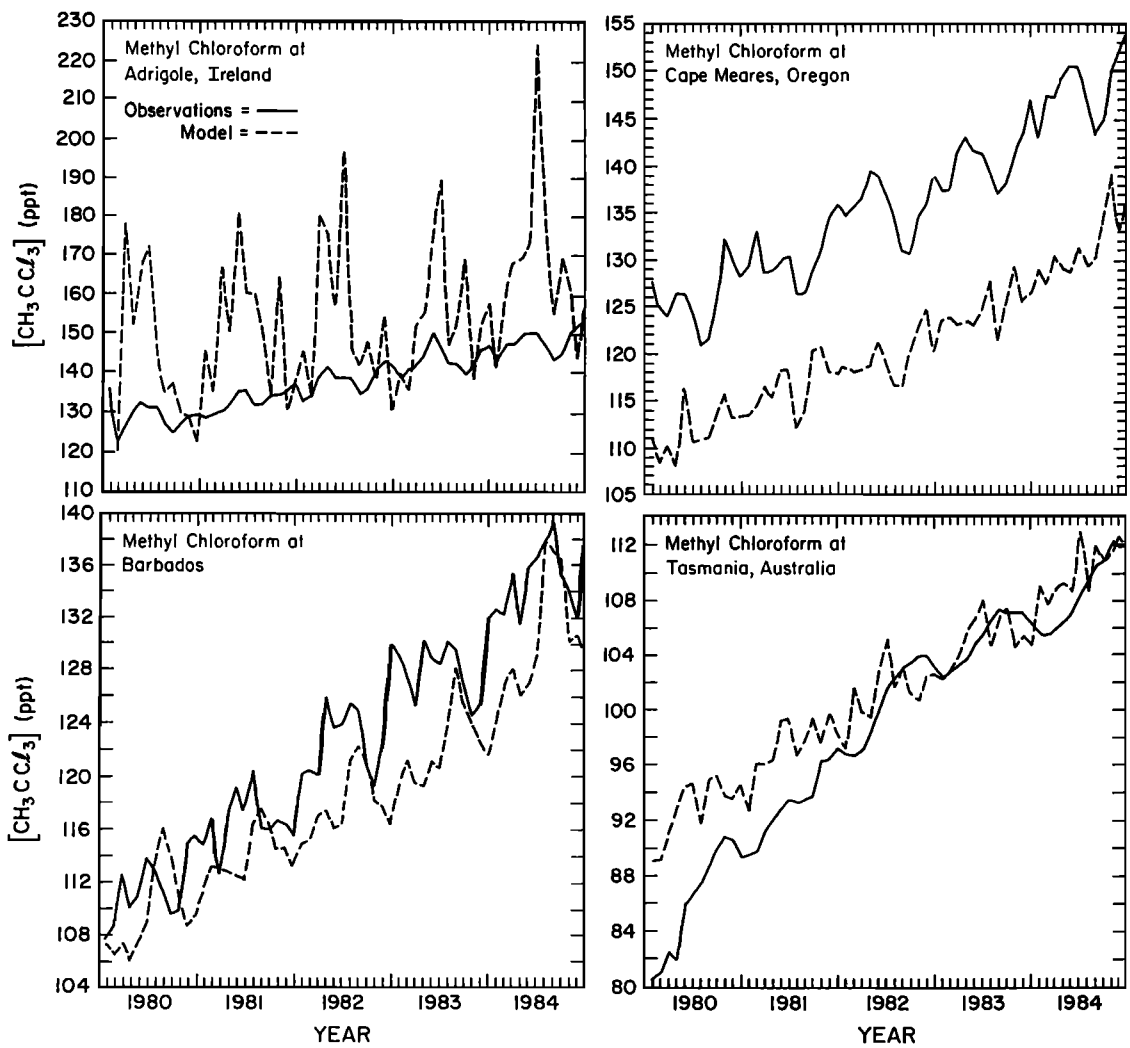

Fig. 7. Methyl chloroform concentrations recorded at four ALE sites for the period 1980–1984 as reported by *Prinn et al.* [1987] along with corresponding model predictions.

predictions with the unselected observations (see Figure 1 of *Prather* [1985]) where methyl chloroform concentration measurements exceed 300 ppt before data selection. Regardless of these problems, the model correctly predicts the long-term trend and the key features of the seasonal cycle at Adrigole, through considerably amplified in comparison to the observations.

At Cape Meares, Oregon, observed concentrations are offset about 10 ppt above the model predictions and share a similar mean concentration as that at Adrigole, Ireland. Model predictions also show less variability than the observed concentrations. It would appear that a source of methyl chloroform located near Cape Meares has not been included in the model or that existing sources are too small. The summer minimum, associated with loss of methyl chloroform to reaction with hydroxyl radicals, is correctly reproduced by the model as is the long-term trend.

At Barbados, model predictions and observations agree reasonably well. The annual minima and maxima are correctly modeled as is the long-term trend.

At Cape Grim, Australia, agreement between model predictions and observations improves in the latter part of the model simulation run. The model predictions show greater variability than the observations. Again, Cape Grim was considered to experience pollution events [*Prinn et al.*, 1983*a*, *b*] and data selection was employed by *Prinn et al.* [1983*a*] to remove these effects to obtain the background behavior of methyl chloroform concentrations over the southern oceans. As a comparison then Figure 8 shows the observed concentrations at Cape Grim along with model predictions corresponding to the model grid over Kaitorete Spit, New Zealand. Model predictions now more closely follow the seasonal variation in the observations. Less variability is also evident in the model predictions at New Zealand than Cape Grim. The minimum methyl chloroform concentration at Cape Grim occurs when the hydroxyl radical concentrations are at maxima in summer.

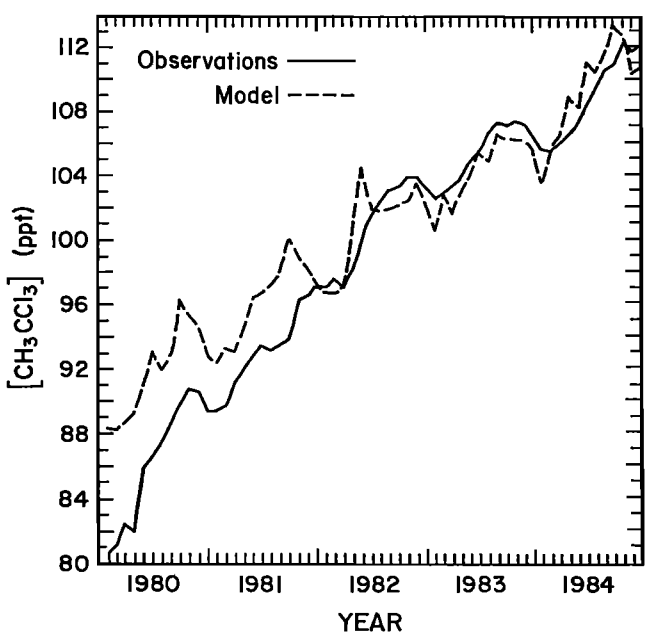

Fig. 8. Methyl chloroform concentrations recorded at Cape Grim, Australia, with model predictions corresponding to a model grid over New Zealand.

Figure 9 shows the zonally and yearly averaged latitudinal gradient predicted by the model averaged over lowest 75 hPa of the troposphere for 1984. Peaks in concentration occur at midnorthern latitudes and to a much lesser extent at 30° south corresponding to the releases of methyl chloroform. A strong latitudinal gradient is predicted in the northern hemisphere with far less variation in concentration in the southern hemisphere as would be expected from the distribution of sources of methyl chloroform.

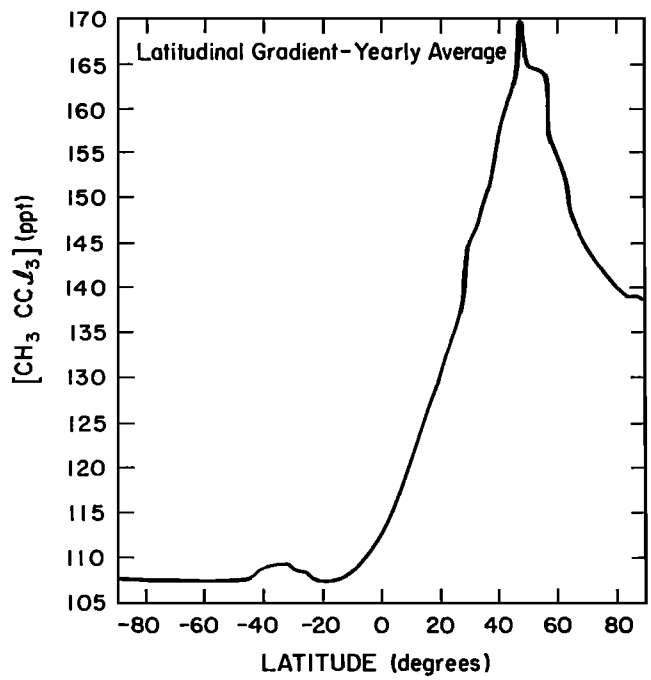

Fig. 9. The annual averaged zonal latitudinal gradient in methyl chloroform computed for the model surface layer for the year 1984.

Figure 10 shows the two-dimensional zonal averaged plot of model predicted methyl chloroform concentrations for January and July 1984. The predicted vertical gradient in concentration is in excellent agreement with available observations [*Rasmussen and Khalil*, 1982].

Figure 11 shows the variation in concentration, averaged over the model surface layer, 75 hPa, with time for 1984. The drop in methyl chloroform concentrations during the last months of the year is most likely associated with the higher average hydroxyl concentrations in the southern hemisphere than the northern hemisphere.

SOURCES OF METHANE RELEASED TO THE ATMOSPHERE

Cicerone and Oremland [1988] have conducted an extensive study of the biogeochemical aspects of atmospheric methane. They included a list of known sources of methane released to the atmosphere along with estimates of the magnitude of those releases and their likely ranges. Table 5 lists known sources of releases of methane to the atmosphere and their magnitudes as determined by *Cicerone and Oremland* [1988], along with the ratio of the source to its estimated range of uncertainty. Their best

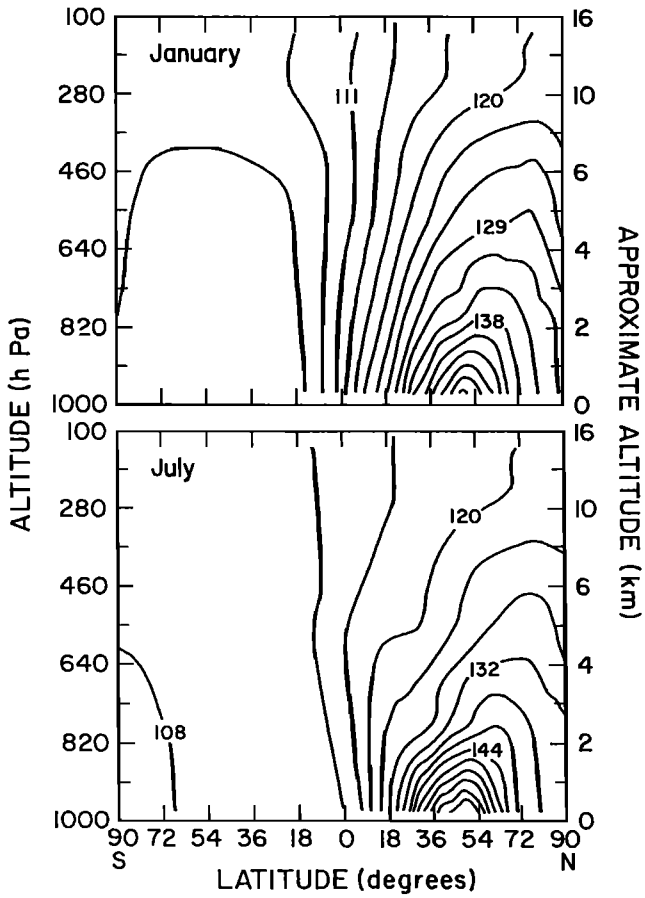

Fig. 10. Model predicted zonally averaged methyl chloroform concentrations (ppt) for the months of January and July 1984.

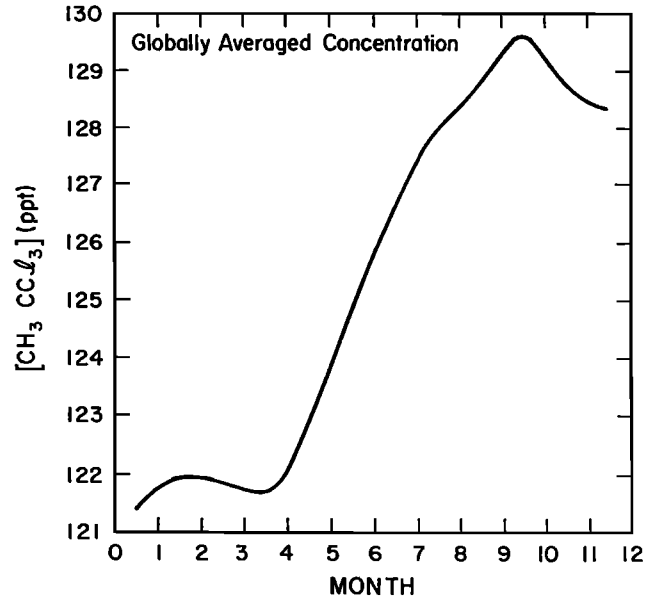

Fig. 11. Variations with time of the globally averaged model surface layer methyl chloroform concentration.

estimate of the global annual steady state source totaled 500 ± 95 × 10^{12} g CH_4. The current annual source probably exceeds this steady state source by 40 or 45 × 10^{12} g/yr. While the total global release of methane can be constrained to within ±20% individual source releases could only be estimated to within about a factor of 2 at best. The larger uncertainty associated with individual sources can be maintained within the constraint of the global total simply by shifting the annual release of methane among the individual sources.

In this study we shall develop two methane source functions which employ the categories for the release of methane to the atmosphere identified by *Cicerone and Oremland* [1988]. While we shall be investigating the total amount of methane released to the atmosphere consistent with the known sinks, which will require adjustment of the total amount released, the individual sources will be adjusted in proportion to the change in the total methane emission. In view of the large uncertainty associated with all the individual source estimates, such an approach is reasonable. Table 11 summarizes the source functions, which are described in the following sections. Source function 2 (SF2) is that of Cicerone and Oremland after multiplying each source by 611/540.

Methane Emissions from a Net Primary Productivity Model

We employ a model of net primary productivity (NPP) of the biosphere to estimate the relative spatial and temporal distribution of methane emitted to the atmosphere from enteric fermentation, natural wetlands, rice paddies, biomass burning, and termites. Here the NPP is defined as photosynthesis minus respiration. The underlying assumption is that some fraction of the NPP of the biosphere decays under anaerobic conditions to produce methane which is then released to the atmosphere. Hence at longitude i, latitude j, and time t we compute the flux of methane $f_{ijt}^{CH_4}$ as

$$f_{ijt}^{CH_4} = \alpha_{ijt} NPP_{ijt} \tag{10}$$

where NPP_{ijt} is the amount of dry organic matter synthesized per unit area of the Earth's surface per unit time and α_{ijt} is the fraction of NPP emitted to the atmosphere.

For the first term of (10), α_{ijt}, very little information is available with which to fix values based on a range of ecosystems. Accordingly, α_{ijt} is fixed as a constant and the distribution of the methane flux to the atmosphere is determined solely as a fraction of NPP. Clearly, measurements of α_{ijt}, at least within the major ecosystems, are needed, recognizing that there are also time delays between photosynthesis and methanogenesis, i.e., that organic material that is converted to methane may be some years old.

NPP has been modeled by relating measured NPP to readily available environmental data such as temperature and precipitation, evapotranspiration, and the length of the growing season [*Lieth*, 1973, 1975]. *Lieth* [1975] has reviewed the above approaches to modeling NPP and presents global maps of NPP based on each model approach. These three approaches generate very similar distributions of NPP. The most significant difference is associated with the NPP model based upon the length of the growing season. This model produces estimates of NPP which vary more strongly with latitude and a zonal variation in NPP which is lower than is generated by the other NPP models. As global temperature and precipitation fields are available as monthly mean gridded data

TABLE 5. Sources of Methane Released to the Atmosphere and Their Magnitude as Estimated by *Cicerone and Oremland* [1988] With the Ratio of the Range to Annual Release

Source	Annual Release 10^{12} g CH_4	Ratio of Range/Release*
Enteric fermentation	80	0.438
Natural wetlands	115	0.870
Rice paddies	110	1.000
Biomass burning	55	0.909
Termites	40	2.25
Landfills	40	1.000
Oceans	10	1.500
Freshwaters	5	4.800
Methane hydrate destabilization	5?	?
Coal mining	35	0.571
Gas drilling, venting, transmission	45	0.555
total	540	

*The range is the estimated span of likely values for each source as determined by *Cicerone and Oremland* [1988].

sets at 2.5° × 2.5° resolution and NPP estimates based on evapotranspiration and the duration of the growing season are similar to that obtained using temperature and precipitation, we have adopted the Miami Model, developed and described in detail by *Lieth* [1973, 1975], which employs temperature and precipitation as the basis for estimating NPP. We shall restrict discussion to the key features of this model.

The Miami model is based upon two simple empirical relationships derived from NPP, precipitation, and temperature data collected at 52 sites representing the world's key ecosystems. The empirical formula derived by *Lieth* [1973, 1975] relating NPP (g dry matter/m^2/yr) to mean annual temperature (°C), T, is stated as

$$NPP_{ij} = \frac{3000}{1 + e^{1.315 - 0.119T}} \tag{11}$$

while the formula relating annual precipitation (millimeters), P, is

$$NPP_{ij} = 3000(1 - e^{-0.000664P}) \tag{12}$$

As two estimates of NPP are computed for each grid point, one value is selected on the basis of the assumption that one factor, either precipitation or temperature, limits NPP. Accordingly, the minimum value of NPP, derived from (11) and (12) above, is adopted as the best estimate of NPP.

Equations (11) and (12) above, as originally developed by *Lieth* [1973, 1975] used annual average values for temperature and precipitation. However, (11) and (12) are very close to linear over most of the range of expected values for temperature and precipitation. By using monthly mean values for temperature and precipitation the month-to-month variation in NPP can be computed. NPP estimates derived using (11) must also be modified to account for the change from annual to monthly averaged data by dividing estimates by 12. This model of NPP implies that during months of lowest rainfall and temperatures, low NPP values will result. During the warm months with high rainfall the largest values of NPP are predicted.

Both precipitation and surface temperature data are available as monthly means on a 2.5° × 2.5° grid. *Oort* [1983] describes the temperature fields. *Shea* [1986] has prepared global maps of precipitation based on a compilation of data from a number of sources covering the period 1950–1979. *Shea* [1986] notes that precipitation data for the southern oceans are particularly unreliable. Fortunately, we only wish to compute NPP using (11) and (12) over the land areas for which the data are most reliable.

Figure 12 shows the distribution of NPP computed for the months January and July. For January the highest values of NPP occur in the southern hemisphere with NPP falling to zero for large areas of the northern hemisphere. In July the situation is reversed with the high values for NPP occurring in the northern hemisphere with small values for NPP accompanying southern hemisphere winter conditions. Table 6 lists the estimates of NPP computed for each month of the year. The highest values occur during the northern hemisphere summer, reflecting the far larger land mass of the northern hemisphere. The number and total area of 2.5° × 2.5° grid cells where either precipitation or temperature were the limiting factors in determining NPP are also listed in Table 6. It should be noted that the number of grid cells does not relate directly to the land area as the area of 2.5° × 2.5° grid cells varies with latitude. A bias toward temperature limiting growth would be expected on the grounds that large numbers of high-latitude grid cells will be temperature limited during winter. The data based on the total area of the grid cells show that precipitation is the limiting factor for the majority of the Earth's surface during most months of the year. Only during the northern hemisphere winter is NPP limited by temperature over a larger land area than is limited by rainfall. The yearly estimate of total NPP computed using (11) and (12) was 129.7 × 10^9 tonnes dry matter, which compares favorably with the estimates derived from other studies as listed in Table 7.

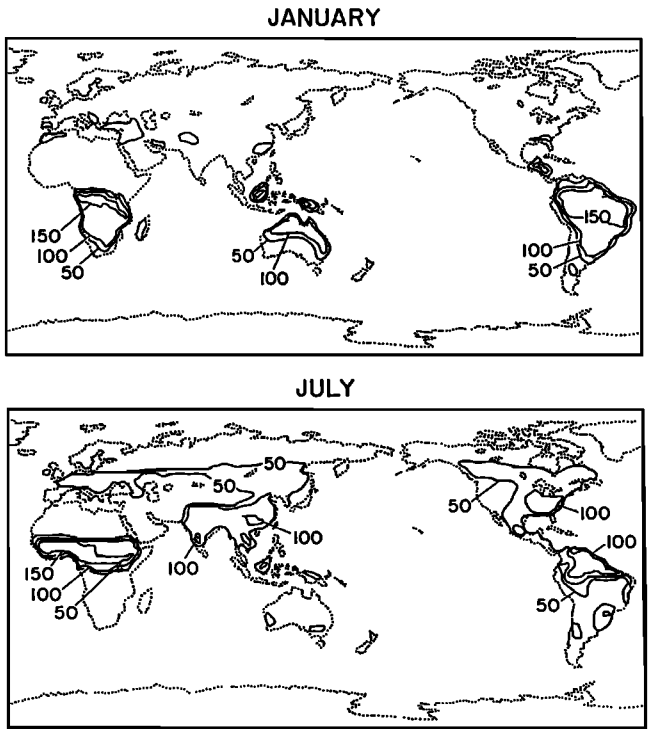

Fig. 12. The spatial distribution of net primary productivity (10^{11} g dry matter) computed for the months of January and July from (11) and (12) as described in the text.

Identifying Methane Source Regions Using Land Cover and Hydrological Data

The net primary productivity model does not identify particular source regions for methane, such as wetlands, and therefore does not allow study of the individual components of the biosphere contributing to the release of methane to atmosphere. Source function 2 includes separate spatial distributions for enteric fermentation, natural wetlands, rice paddies, biomass burning, and termites. To examine these individual contributions requires a far more exhaustive data set at a fine resolution. No data sets are presently available which directly link land cover or land use with measured methane fluxes to the atmosphere. *Matthews and Fung* [1987] have estimated the extent of natural wetlands and computed the methane flux to the atmosphere, while *Lerner et al.* [1988] determined the methane emission from animals. In each case, extensive data on the distribution of these sources of methane emissions were not available. Instead, a compilation of source regions was obtained through the examination of data from a wide range of sources. In many cases it was difficult to evaluate the uncertainties associated with the underlying data sources because of the great variability in the origins, content, purpose of the data collector, resolution, and time of preparation [*Matthews and Fung*, 1987]. For example, *Matthews and Fung* [1987] note that the evaluation of wetland areas is complicated, particularly in tropical regions, by the seasonal variation in inundated areas and whether the information recorded on maps reflects the minimum, mean, or maximum area inundated.

Henderson-Sellers et al. [1986] have examined a number of available global land-surface data sets for use in climate-related studies. In each case the data sets were compiled using different methods. This variation in methodology is reflected in the wide range and number of vegetation types used to classify land cover and the differences in resolution. In no case have these vegetation data sets been prepared with the aim of estimating the flux of methane to the atmosphere.

One source of systematic error associated with these land cover data sets arises from the approach of reporting only the major ecosystem present with a grid cell (>

TABLE 6. Computed NPP by Month of the Year With the Number and Total Area of Grid Cells Where Either Temperature or Precipitation is the Limiting Factor Determining NPP

		Number and Total Area of Grid Cells* Limited by Precipitation		Temperature	
Month	NPP, 10^9 g/month	N	Area, 10^{14} m^2	N	Area, 10^{14} m^2
1	8.91	1101	0.637	1947	0.732
2	8.95	1179	0.668	1871	0.701
3	9.88	1227	0.687	1823	0.682
4	10.67	1529	0.814	1521	0.554
5	11.35	1850	0.877	1200	0.492
6	12.10	2066	0.939	984	0.430
7	13.44	2040	0.901	1010	0.468
8	13.32	1849	0.862	1201	0.507
9	12.17	1675	0.852	1375	0.517
10	10.75	1395	0.791	1655	0.578
11	9.34	1259	0.733	1791	0.636
12	8.83	1106	0.649	1944	0.720
Total	129.71	18278	9.410	18322	7.017

*The grid cells are 2.5° × 2.5° in size.

TABLE 7. Estimates of the Annual Terrestrial Net Primary Productivity (NPP) Obtained in Different Model Studies

NPP, tonnes $\times 10^9$/yr)	Model Basis	Source
124.478	temperature and precipitation	*Lieth* [1975]
118.706	evapotranspiration	*Box* [1975]
73.5	length of growing season	*Lieth* [1975]
120.4	carbon in live vegetation	*Olson et al.* [1983]
129.7	temperature and precipitation	this study

50% land cover). This leads to a systematic underestimation of land cover for an ecosystem that is intermixed with another more dominant ecosystem and systematic overestimation if we assume that the dominant ecosystem represents 100% of the land cover when other ecosystems are present. It is hoped that taken over the globe these effects will average out. One solution to this problem is to increase the resolution of the data set. For this reason land cover data sets of 1° and 0.5° resolution are now common. This approach to the problem of resolution is certainly a good compromise when faced with determining the actual percentage of land cover for each vegetation type within every grid cell.

Other approaches to the problem of properly representing mixed ecosystems include the introduction of additional categories which represent, for example, the intermixing of nonwooded vegetation types with wood or forest cover [*Olson et al.*, 1983]. *Wilson and Henderson-Sellers* [1985] included information on both a primary and a secondary vegetation category. The primary land cover class was considered to represent the land cover that occupies $\geq$ 50% of a 1° × 1° grid area while the secondary land cover represents cover types occupying between 25%–50% of the grid area.

In the modeling study reported here we have employed the data set developed by *Wilson and Henderson-Sellers* [1985]. This data set includes both primary and secondary classifications of land cover, and its land-cover classes could be easily related to methane source regions. In the following discussion we shall refer to these land cover classes in constructing source functions for the release of methane from the biosphere.

Methane Emissions From Biomass Burning

Biomass burning is now recognized as an important source of a number of trace gases, including carbon dioxide, methane, carbon monoxide, nitrogen dioxide, nitrous oxide, and nonmethane hydrocarbons [*Seiler and Crutzen*, 1980; *Crutzen et al.*, 1979; *Fishman et al.*, 1986; *Greenberg et al.*, 1985]. Biomass burning also appears to lead to a substantial photochemical production of tropospheric ozone through the release of ozone precursor compounds [*Crutzen et al.*, 1979; *Delany et al.*, 1985; *Crutzen*, 1987]. Recent measurements of tropospheric ozone in the tropics by *Logan and Kirchoff* [1986] and the analysis of satellite total ozone data by *Fishman et al.* [1986] and *Fishman* [1988] support the conclusion that biomass burning contributes significantly to tropospheric ozone formation.

Biomass burning has been recognized for some time to be a source of atmospheric methane [*Crutzen et al.*, 1979]. However, the spatial distribution, the seasonal pattern, and the magnitude of the emission of methane have been the subject of only a few studies [*Seiler and Crutzen*, 1980; *Crutzen et al.*, 1985; *Crutzen*, 1987]. Given the range of environmental factors which may affect the amount of biomass burnt and the resulting methane emissions, only limited confidence can be placed in current estimates of methane emissions from biomass burning.

In order to construct a spatial and temporal distribution for the release of methane independent of NPP the land cover information of *Wilson and Henderson-Sellers* [1985] has been used to identify regions where biomass burning occurs. These regions are tropical savanna, tropical grassland plus shrub, open tropical woodland, tropical pasture, thorn shrub, and cane sugar (codes 37, 32, 23, 33, 28 and 43 as listed by *Wilson and Henderson-Sellers* [1985]). To distribute the flux of methane from biomass burning, a simple model based on precipitation was constructed. It was assumed that the flux of methane from burning varied inversely with respect to precipitation. On the basis of these assumptions the flux of methane attributed to biomass burning at each grid cell with longitude i, latitude j and month t was computed as follows

$$f_{ijt}^{CH_4} = f_{ij}^{CH_4}[P_{ij}^{tot}/P_{ijt}]/[\sum_{t=1}^{12}(P_{ij}^{tot}/P_{ijt})] \qquad (13)$$

where P is precipitation (mm), P_{ij}^{tot} is the annual precipitation in that grid square, and $f_{ij}^{CH_4}$ is the estimated annual total release of CH_4 to the atmosphere from biomass burning at that grid cell.

Figure 13 shows the distribution of the flux of methane computed using (13) for the months of March when, based on ozone measurements [*Fishman*, 1988], biomass burning over South America should be at a minimum, and October, when biomass burning has been observed to be at its maximum over the savannas of Africa and South America. Note also that the model predicts a significant contribution to methane emissions from biomass burning over South East Asia and the tropical north of Australia, as would be expected [*Seiler and Crutzen*, 1980]. Figure 14 shows the computed annual averaged latitudinal distribution of the flux of methane to the atmosphere from biomass burning averaged over 2.5° latitudinal bands.

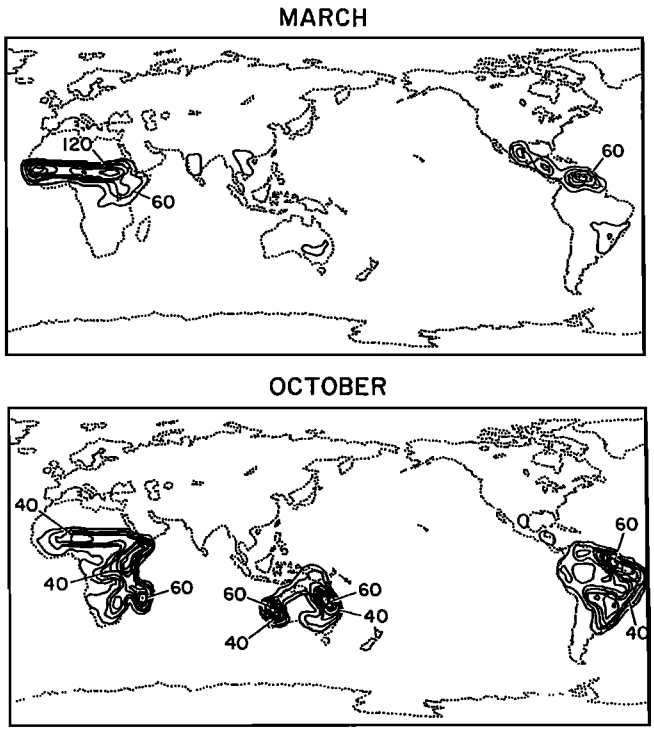

Fig. 13. The calculated spatial distribution of the flux of methane (10^8 g CH_4 per 2.5° x 2.5° grid square) from biomass burning computed using (6) for the months of March and October.

Figure 13 shows that methane released from biomass burning has been confined to the tropics. Clearly, biomass burning also occurs at higher latitudes, however, the frequency and extent of biomass burning at higher latitudes is such that only a very small release of methane occurs as a consequence of biomass burning, when compared with the tropical releases. *Seiler and Crutzen* [1980] estimated that the biomass burnt annually in temporal and boreal forests represented ~ 4% of the total annually burned biomass.

TERMITES

Termites are known to emit methane as a result of digestion. Several estimates of total annual methane production have been derived. These estimates are listed in Table 8. *Zimmerman et al.* [1982], based on field and laboratory measurements of methane emissions from termites, estimated that the annual release of methane to the atmosphere by termites, assuming that termites consume an average of 28% of available NPP, was as high as 151.6 × 10^{12} g methane. However, much uncertainty has surrounded this original estimate of methane production. More recent estimates indicated that much lower values for methane releases by termites should be expected. *Collins and Wood* [1984] attacked the basis for *Zimmerman et al.* [1982] estimates. However, *Zimmerman et al.* [1984] defended the basis for their original estimate of methane production by termites. Field measurements by *Seiler et al.* [1984] led to much lower estimates of the release rate of methane from termite nests. These results stand in contrast to the values estimated by *Rasmussen and Khalil* [1983], who estimated methane emissions from termites would lie in the range 10–100 × 10^{12} g CH_4 yr. Clearly, much uncertainty surrounds the estimate of the total global methane emission from termites due to the limited number of field and laboratory measurements and the difficulty of extrapolating such measurements to the global scale. In view of the large uncertainties associated with estimates of the flux of methane from other biogenic sources such as wetlands, rice paddies, and enteric fermentation, as noted by *Cicerone and Oremland* [1988], all published estimates of the flux of methane from termites can be accommodated within the range of total methane source budgets that have been prepared to date. *Cicerone and Oremland* [1988] note these problems associated with estimating methane emissions from termites and, as listed in Table 5, suggested a value of ~ 40 × 10^{12} g CH_4 yr, essentially a median value of available estimates.

In order to construct a global distribution of methane emissions independent of NPP the detailed land cover data of *Wilson and Henderson-Sellers* [1985] have been combined with estimates of methane emissions from a range of ecological regions determined by *Zimmerman et al.* [1982]. Table 9 lists the estimated flux of methane from termites as derived from the data of *Zimmerman et al.* [1982], expressed in units of grams per unit area per year, for each of the ecological regions identified by *Zimmerman et al.* [1982]. The flux values of *Zimmerman et al.* [1982] were used to scale the contribution of the different ecological regions to the total methane emission, as listed in Table 10. For each ecological region a number of land cover codes [*Wilson and Henderson-Sellers,* 1985] have been assigned a methane flux attributed to termite activity. Unfortunately, the direct assignment of the land cover codes of *Wilson and Henderson-Sellers* [1985] to

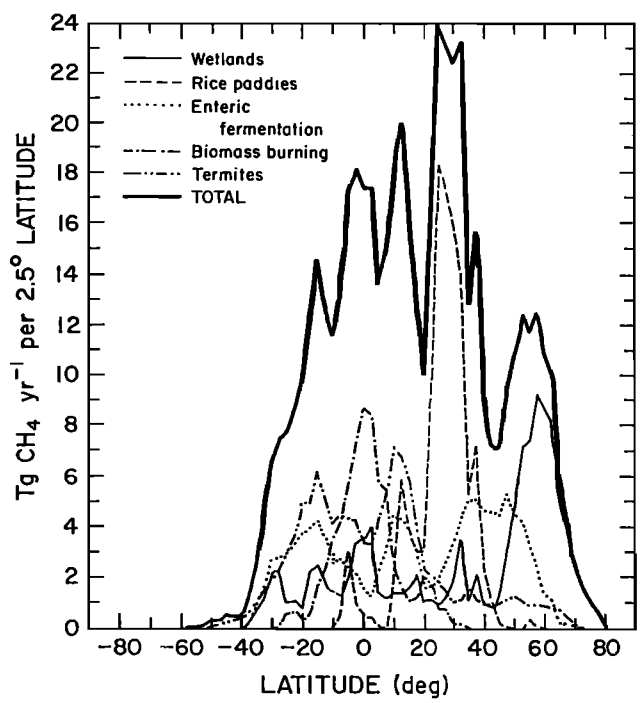

Fig. 14. Latitudinal distribution of the flux of methane from rice paddies, biomass burning, natural wetlands, termites, and enteric fermentation averaged over 2.5° latitudinal bands.

TABLE 8. Estimated Total Annual Global Methane Released to the Atmosphere by Termites

Methane Emission, 10^{12} g CH_4	Source
151.6	*Zimmerman et al.* [1982]
2–5	*Seiler et al.* [1984]
~15–37.9	*Collins and Wood* [1984]*
50	*Rasmussen and Khalil* [1983]

* *Collins and Wood* [1984] suggest that global consumption estimates of NPP used by *Zimmerman et al.* [1982] should be reduced by a factor of 4–10.

the ecological regions of *Zimmerman et al.* [1982] is not entirely straightforward. In particular, assigning methane emissions in temperate regions proved difficult. Rather than use a separate methane flux for temperate forests and for wood/shrub a single value, the mean of the two methane flux values was adopted. No methane emissions from temperate grasslands were included as temperate grasslands were not explicitly identified in the *Wilson and Henderson-Sellers* [1985] data base. This implies that the flux of methane may be underestimated from temperate regions by a few percent. Table 11 lists the land cover codes of *Wilson and Henderson-Sellers* [1985] and their associated methane flux. With the land area associated with each land cover category within each grid cell based on the *Wilson and Henderson-Sellers* [1985] data and the methane flux data of Table 10 the yearly total methane flux within each model grid cell was computed as follows.

$$f_{ij}^{tot} = A_l e_k \tag{14}$$

where A_l is the land area (meters squared) associated with land cover type, l, within a grid cell at longitude, i, and latitude, j, and e_k represents the methane emission rate corresponding to the land cover code, l, as listed in Table 11. Figure 15 shows the spatial distribution of the annual total flux of methane to the atmosphere derived from termites. Figure 14 includes the annual average latitudinal distribution of methane emissions from termites.

A seasonal variation in methane flux from termites was modeled as a function of the month-to-month variation in NPP. Hence the flux of methane from termites, $f_{ijt}^{CH_4}$ in each grid cell of longitude, i, latitude, j, at month t was computed as

$$f_{ijt}^{CH_4} = f_{ij}^{tot}\left[NPP_{ijt}/\sum_{t=1}^{12} NPP_{ijt}\right] \tag{15}$$

where NPP_{ijt} is the net primary productivity and f_{ij}^{tot} is the annual total methane emission at each grid cell. This representation of the seasonal cycle of methane emissions may lead to too large a seasonal cycle at higher latitudes. However, the methane emission from termites at these latitudes is small.

TABLE 9. Methane Fluxes to the Atmosphere Attributed to Termites With Different Land Cover Categories

Ecological Regions	Methane Flux*, g/m^2/yr
Tropical wet forest	0.63
Tropical moist forest	2.83
Tropical dry forest	2.01
Temperate forest	0.38
Wood/shrub	0.27
Wet savanna	2.81
Dry savanna	0.54
Temperate grassland	1.38
Cultivated	1.82
Desert scrub	0.16

*Methane fluxes were derived from *Zimmerman et al.* [1982].

TABLE 10. Methane Fluxes Assigned to the Land Cover Classes of the *Wilson and Henderson-Sellers* [1985] Land Cover Data Base

Land Cover Code	Methane flux, g/m^2/yr
10, 11, 12, 13, 14, 16, 17, 18, 19, 20, 21, 22, 24, 27, 28, 30, 31, 35, 39	0.325
34, 36	0.54
50	0.63
40, 41	1.82
23, 25, 26	2.01
32, 33, 37	2.81
51, 52	2.83

METHANE EMISSIONS FROM RICE PADDIES

The first estimates of methane emissions from rice paddies were based upon laboratory measurements of methane fluxes by *Koyama* [1963]. When extrapolated globally these measurements lead to estimates of the flux of methane to the atmosphere of 280 Tg CH_4 yr^{-1} [*Ehhalt and Schmidt,* 1978]. However, the first field measurements of methane emission rates by *Cicerone and Shetter* [1981] resulted in a much lower estimate of the global flux of methane of 59 Tg CH_4 yr^{-1}. Another lower estimate of the global flux of methane from rice paddies has been published by *Seiler et al.* [1984], 35–59 Tg CH_4 yr^{-1}. *Holzapfel-Pschorn and Seiler* [1986] correlated methane emanating from an Italian rice paddy with soil temperature to predict a global total annual methane emission from rice paddies of 66.7–166.3 Tg CH_4 yr^{-1}. *Holzapfel-Pschorn and Seiler* [1986] also computed the change in methane released for the period 1940–1979 based upon statistics for the annually harvested rice paddy area data collected by the United Nations Food and Agricultural Organization. They found that the computed methane emission from rice paddies, averaged

TABLE 11. Summary of the Methane Source Functions Used in the Model Studies

Source Function 1		Source Function 2	
Source Distribution	Flux, 10^{12}g CH_4 yr^{-1}	Source Distribution	Flux, 10^{12}g CH_4 yr^{-1}
NPP (includes methane from enteric fermentation, natural wetlands, rice paddies, biomass burning and termites)	473.5	enteric fermentation	92.2
		natural wetlands	132.5
		rice paddies	126.8
		biomass burning	63.4
		termites	46.1
Fossil Fuels and Landfills (includes methane from coal mining, gas drilling and	138.3	fossil Fuels and Landfills (includes methane from coal mining, gas drilling)	138.3
Oceans	11.5	oceans	11.5
Total	623.3		610.8

SF1 assumes that the biospheric emissions of methane are proportional to net primary productivity. SF2 is that of Cicerone and Oremland except that each of their sources has been multiplied by 611/540. (See text for detailed descriptions.)

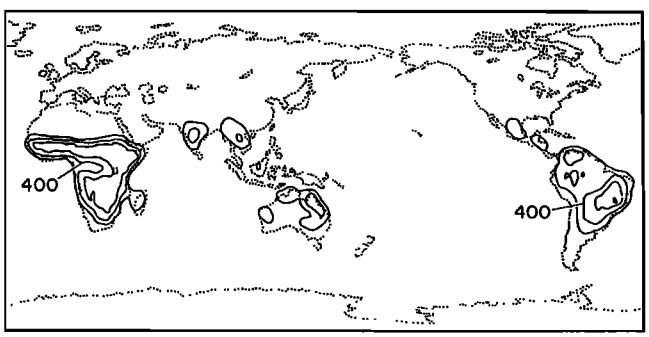

Fig. 15. Annual total flux of methane (10^8 g CH_4 per 2.5° x 2.5° grid square) to the atmosphere derived from termites.

over the last 35 years, has been increasing at about 1.6% per year. It should be noted that consideration of the flux of methane from the land areas prior to conversion to rice paddies was not considered by *Holzapfel-Pschorn and Seiler* [1986]. If this area were a swamp prior to becoming a rice paddy then very little change in the methane flux to the atmosphere would have occurred and the net flux of methane to the atmosphere would have remained relatively constant over time. If, on the other hand, rice paddies replaced dry unproductive land, a dramatic increase in the methane flux would have occurred. Clearly, then, if the net increase in the methane flux to the atmosphere from rice paddies or any other agricultural practice is to be determined the flux of methane to the atmosphere prior to the introduction of rice paddies or other agricultural practice must be estimated.

In the study reported here, source regions for methane from rice paddies, independent of the NPP model, have been identified using the global archive of land cover and soils data developed by *Wilson and Henderson-Sellers* [1985]. This data set includes a land cover category specifically for paddy rice. Both primary and secondary land cover data sets have been employed at the 1° × 1° resolution to estimate the total land surface in each of the 2.5° × 2.5° atmospheric model surface grids. The calculated total surface area of rice paddies derived from the *Wilson and Henderson-Sellers* [1985] data is 1.82 × 10^{12} m^2. The nature of the data sets employed to determine the source of methane from rice paddies is such that if rice paddies constitute less than 25% of the total land area of a 1° × 1° cell [*Wilson and Henderson-Sellers*, 1985], no flux of methane from rice paddies will be included. Using land cover data sets which include only the major ecosystem within each grid cell will lead to the underestimation of the total land area. Fortunately, rice paddies are not widely scattered, which would lead to a severe underestimation of the area of rice paddies. The estimate of the global total land area of rice paddies, 1.82 × 10^{12} m^2 based on data from a large number of sources, is ~20% higher than that employed by *Holzapfel-Pschorn and Seiler* [1986]. Since *Holzapfel-Pschorn and Seiler* [1986] based their estimate upon a single source of information, the United Nations Food and Agricultural Organization, it is not surprising that a lower estimate would result.

Emissions of methane have been distributed uniformly over the total rice paddy area. Figure 16 shows the spatial distribution of the annual total flux of methane

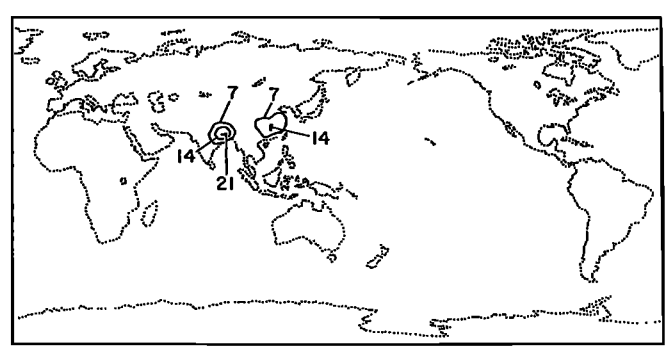

Fig. 16. Annual total flux of methane (10^{11} g CH_4 per 2.5° x 2.5° grid square) from rice paddies.

to the atmosphere from rice paddies. Figure 14 shows the latitudinal distribution of the flux of methane from rice paddies and other large methane sources. Seasonal variation was determined according to the ratio of the NPP computed for each month at each grid cell to the total NPP for the year within each grid cell following (15). This approach to the seasonality of the methane flux from rice paddies leads to a single peak in the flux of methane in midsummer. The measurements of *Cicerone et al.* [1983] and *Holzapfel-Pschorn and Seiler* [1986] indicate that two peaks in the methane flux occur. These peaks in methane flux occur during the tillering of the rice paddies and when the rice plants are flowering. However, the data of both *Cicerone et al.* [1983] and *Holzapfel-Pschorn and Seiler* [1986] are not conclusive as to whether the same seasonal pattern applies everywhere. Also, as the data of both *Cicerone et al.* [1983] and *Holzapfel-Pschorn and Seiler* [1986] do not represent large area averages, the effect of areal averaging may lead to a single peak in the methane flux from rice paddies, but in reality we do not yet know how these methane emissions vary during the growing season.

Methane Emissions from Natural Wetlands

A number of data bases are available which include the extent of natural wetlands. Both *Wilson and Henderson-Sellers* [1985] and *Olson et al.* [1983] include a code for natural wetlands in their respective data bases. Both of these data bases only provide estimates of the extent of natural wetlands when natural wetlands are either the primary or secondary land cover within each grid cell. Unfortunately, as wetlands are widely scattered this approach to estimating the extent of natural wetlands leads to a systematic bias toward underestimation.

To overcome this problem, *Cogley* [1985] developed a data base for natural wetlands, THYDRO, at a $1° \times 1°$ resolution in which the percentage of natural wetlands within each grid cell has been evaluated. Using the data of *Cogley* [1985], the total area of natural wetlands was computed to be 4.96×10^{12} m^2. This value compares well with that derived by *Matthews and Fung* [1987] of 5.26×10^{12} m^2 supporting their hypothesis that earlier studies attempting to estimate the flux of methane from wetlands had probably employed a value for the extent of natural wetlands that was a factor of 2 too small.

Mathews and Fung [1987] also computed the global annual emission of methane to the atmosphere based on the division of wetlands into five major wetland ecosystems, namely, forested bogs, nonforested bogs, forested swamps, nonforested swamps, and alluvial formations, an estimate of the typical ecosystem flux and the duration of the CH_4 release [*Matthews and Fung*, 1987].

Using the area and emission rate data for each major ecosystem, as listed by *Matthews and Fung* [1987], the product of these two values were computed giving a total methane emission rate per day for each ecosystem. The results for forested bog, nonforested bog, forested swamp, nonforested swamp, and alluvial formations were 415.4, 179.4, 76.09, 120.96, and 5.82×10^9 g CH_4 day^{-1}, respectively. The product of the total area of each major wetland ecosystem and its flux of methane, while ignoring the variation in length of production season, gives some indication of the relative importance of each of the major ecosystems. Clearly, the forested and nonforested bog represent the most significant source of methane from wetlands, whereas alluvial formations are anticipated to play a minor role. However, it should be noted that estimates of the methane emission rates from the major ecosystems are based upon a limited number of measurements which are subject to considerably uncertainty. *Cicerone and Oremland* [1988] noted that such factors as soil water levels, temperatures, and possible seasonal variations in methanogenic pathways are significant in determining the flux of methane from wetlands [see *Harriss et al.*, 1982; *Crill et al.*, 1988; Whalen and Reeburgh, 1988].

Matthews and Fung [1987] calculated the latitudinal distribution of methane emissions and the area of natural wetlands. The primary difference between the latitudinal distribution of wetland area and methane emissions lies in the slightly larger methane emission at high northern latitudes relative to the methane emission from tropical regions than is indicated by wetland area alone. The dominance of forested and nonforested bogs at high northern latitudes and forested and nonforested swamps at equatorial latitudes, as found by *Matthews and Fung* [1987], causes this difference.

Figure 14 shows the latitudinal distribution of the methane flux from wetland areas derived from the THYDRO wetland area data set of *Cogley* [1985]. These data of *Cogley* [1985] lead to a latitudinal distribution of the flux of methane from wetlands with a slightly greater emphasis on tropical regions than that obtained by *Matthews and Fung* [1987]. Figure 17 shows the geographical distribution of the annual total methane emissions from wetlands. The distribution of methane emissions from wetlands presented in Figure 17 is qualitatively similar to that obtained by *Matthews and Fung* [1987]. As the distributions of wetlands are similar, the difference in the latitudinal distribution of methane fluxes between *Matthews and Fung* [1987] and our results is attributed to the difference in the flux rates assigned by *Matthews and Fung* [1987] to swamps and bogs. The seasonal emissions of methane from wetlands were distributed in proportion to NPP following the method of (15).

Aselmann and Crutzen [1989] have recently determined the distribution of natural wetlands and rice paddies at a resolution of 2.5° latitude × 5° longitude. They obtained a total wetland area of 5.7×10^6 km^2. This value is larger than the value obtained using the THYDRO data set and also that of *Matthews and Fung* [1987]. The differences between the three data sets represent the

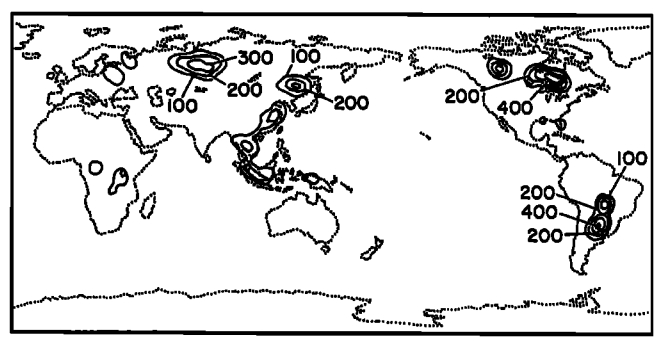

Fig. 17. Annual total flux of methane (10^9 g CH_4 2.5° x 2.5° grid square) to the atmosphere from wetlands as derived from existing data and used in the model.

difficulties associated with the clear definition of wetland regions in the source data used to compile the geographical distributions. A detailed intercomparison of the three data sets combined with actual field measurements would be necessary in order to resolve the differences in the estimated spatial distributions of wetlands. However, it should be recalled that the uncertainties associated with the methane emissions from the source regions are also large.

METHANE EMISSIONS FROM ENTERIC FERMENTATION

Methane is produced as a byproduct of digestion in animals as a consequence of the microbial activity of bacteria present within the animal gut [*Hungate*, 1966]. While a number of studies have reported estimates of methane released from enteric fermentation [*Ehhalt*, 1974; *Crutzen*, 1983; *Seiler*, 1984; *Khalil and Rasmussen*, 1983; *Sheppard et al.*, 1982] two recent studies have considered the problem of estimating methane emissions from enteric fermentation in detail. *Crutzen et al.* [1986] derived an estimate of the annual global flux of methane from cattle, buffalos, sheep, camels, mules and asses, pigs, and horses of 78 $\times$ 10^{12} g CH_4 yr, with an uncertainty of about 15%, using separate methane emission rates for cattle, sheep, and pigs located in either developed or developing countries. This distinction was employed because the known variation in methane production from animals associated with the quality and quantity of the food intake.

Lerner et al. [1988] constructed a global 1° $\times$ 1° resolution data base of methane emissions arising from enteric fermentation. They employed Food and Agricultural Organization statistical data on animal populations, as *Crutzen et al.* [1986] did, and deduced similar methane emission rates from individual animals though with more detailed assumptions concerning the spatial distribution of emission rates. *Lerner et al.* [1988] computed an annual global methane flux of 75.8 $\times$ 10^{12} g CH_4 yr^{-1}.

In the study reported here the distribution of the flux of methane from animals is based on a simple model. Using the land cover codes of *Wilson and Henderson-Sellers* [1985], land cover categories likely to support agricultural activity were identified. The land cover categories, a description of which appears in the work by *Wilson and Henderson-Sellers*, were codes 13, 16, 21, 23, 24, 26, 27, 31, 32, 33, 34, 35, 36, 37, 39, 40, and 41. The total annual methane emission from enteric fermentation was then distributed uniformly with respect to the total land area. Figure 18 shows the global distribution of the annual total flux of methane arising from enteric fermentation. Figure 14 includes the annual average latitudinal distribution of methane emissions from enteric fermentation. Comparing Figure 14 with the results obtained by *Lerner et al.* [1988] indicates that *Lerner et al.* [1988] predict a larger methane emission in high northern latitudes than shown in Figure 14. However, given the uncertainty associated in evaluating methane emissions over different geographical regions as noted by *Crutzen et al.* [1986] and the problems associated with distributing the animal populations, the latitudinal distributions are not inconsistent.

The seasonal variation of methane emissions from enteric fermentation was modeled assuming that the emissions are proportional to NPP within each grid cell according to (15) rather than using animal populations because of the difficulty of obtaining reliable estimates of animal population as a function of month on a 2.5° $\times$ 2.5° grid. Relating methane emissions to NPP is the basis of the assumption that, coincidentally, the majority of new births occur in the spring and the majority of animal slaughtering occurs in the autumn and winter. Assuming that NPP is related to methane emissions from enteric fermentation may lead to overestimation of the seasonality at higher latitudes where NPP will fall to near zero in winter, whereas animal herds will be maintained at some fraction of their summer levels.

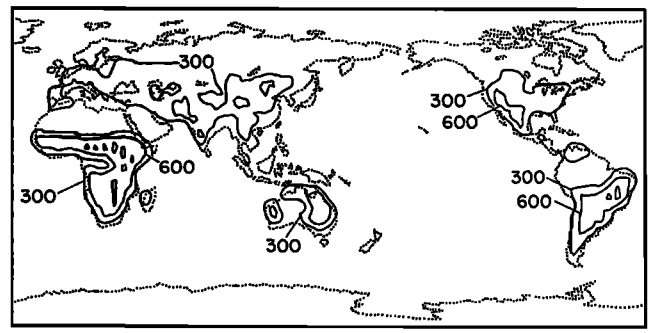

Fig. 18. The spatial distribution of the flux of methane (10^8 g CH_4 per 2.5° x 2.5° grid square) to the atmosphere from enteric fermentation.

FOSSIL FUEL AND LANDFILL RELEASES OF METHANE

Fossil fuel releases of atmospheric methane are associated with coal mining and gas drilling and venting rather than from the combustion of fossil fuels, as is the case with CO_2. However, both coal mining and gas drilling are often located near fossil fuel power plants and hence fossil fuel releases of CO_2. The major exception being the venting of unburnt methane from the flaring of natural gas associated with oil and gas exploration and recovery, particularly offshore activities [*Cicerone and Oremland*, 1988]. However, the total methane released from these latter activities is currently thought to be small at around 14 $\times$ 10^{12} g CH_4 yr^{-1} or less, and methane emission estimates from individual exploration and production facilities are lacking, making it difficult to develop a source function for the spatial distribution of methane from coal mining and gas drilling and venting. As better information becomes available on this source of methane it shall be incorporated into the model.

It should be noted that in regard to the fraction of the total release of methane attributed to fossil fuels, analysis of ^{14}C isotope measurements of methane can provide an independent estimate of the fossil fuel source of methane. *Lowe et al.* [1988] and *Wahlen et al.* [1989] have used such an approach to estimate the fossil fuel component of atmospheric methane. They found that methane from fossil fuels could be as much as 50% higher than is indicated in Table 5. Alternatively, *Cicerone and Oremland* [1988] have suggested that biological sources of ^{14}C depleted methane from old organic matter may explain the unexpectedly low atmospheric $^{14}CH_4$ measurements.

Methane may be released from landfills in amounts that are globally significant but existing estimates are

uncertain [*Bingemer and Crutzen,* 1987]. *Cicerone and Oremland* [1988] noted that further work with regard to landfill emissions of methane is required in the areas of the amounts of waste material and trends, composition of waste material, landfill management practices, and the impact of methane oxidation and burning. Little data are available regarding the spatial distribution of the flux of methane from landfills. Landfills are associated with populated areas of industrial countries. *Bingemer and Crutzen* [1987] have estimated that the majority of methane released from landfills (78%) is from industrial countries.

Accordingly, to model the spatial distribution of fossil fuel and land fill releases of methane to the atmosphere, their combined emissions have been assigned a single spatial distribution. Fossil fuel emissions of CO_2 have been comprehensively studied [*Marland et al.,* 1985; *Rotty,* 1987*a*, *b*]. The approach adopted then, is to model methane emissions from fossil fuels and landfills in proportion to the release of CO_2 from fossil fuel combustion.

Estimates of the fossil fuel emissions of CO_2 were those of *Marland et al.* [1985]. Using CO_2 emission estimates for 1980, they generated a $5^\circ \times 5^\circ$ grid of CO_2 emissions expressed as a fraction of the total annual CO_2 emission from fossil fuel. By substituting a total methane emission the spatial distribution of methane releases from coal mining, gas drilling, and venting, and landfills may be approximated. Clearly, as more comprehensive information on the spatial distribution of methane released from fossil fuel production and landfills becomes available, the modeled spatial release can be modified.

No seasonal cycle for these releases was incorporated into the model. This assumption is most likely valid for the release of methane from coal mining and oil and gas drilling where production quotas and equipment do not follow strong seasonal cycles. Fossil fuel combustion, which would be expected to follow a stronger seasonal cycle, has been observed by *Rotty* [1987*b*] to have only a small seasonality. Methane from landfills may exhibit a seasonality with changing air temperatures. However, thermal insulation below the surface ground layer and heat produced from the degradation of the landfill material may act to minimize the seasonality in the release of methane.

Methane Released From the Oceans

Cicerone and Oremland [1988] have reviewed the available data for methane released to the atmosphere by the oceans. The estimate of this flux was derived from the work of *Ehhalt* [1974]. They found that the original data employed by *Ehhalt* [1974] was limited and was obtained when 15–20% less methane was present in the atmosphere compared with present-day methane concentrations. *Cicerone and Oremland* [1988] suggest that the flux of methane from the ocean to the atmosphere has reduced greatly, or even reversed in sign, and recommend that extensive sampling of marine surface waters be undertaken.

We adopt the value reported by *Cicerone and Oremland* [1988] for the flux of methane from the oceans to the atmosphere. However, we caution that this estimate may require substantial revision if new measurements of the flux of methane from the oceans to the atmosphere should become available. Fortunately, such a large uncertainty is associated with only a small source of methane.

The exchange of methane between the ocean and atmosphere is modeled as a uniform release of methane from the oceans. This simple model may not be appropriate for the continental shelf regions where the flux of methane to the atmosphere may be considerably higher per unit area than over the open ocean [*Ehhalt,* 1974]. However, given the small magnitude of the source and the lack of reliable measurement data distinguishing between the release of methane from the open oceans and the continental shelf regions, a more complex model for the release of methane from the oceans does not seem warranted.

No seasonality in the release of methane to the atmosphere from the oceans has been included in the model. Instead, a constant release rate over time has been assumed. Again, lack of sufficient data and the small magnitude of the source do not warrant the development of a more sophisticated model of the seasonality of the release of methane from the oceans at this time.

Perhaps the most important measurements of the flux of methane from the oceans would be a comparison of the fluxes from the open oceans and continental shelf regions. It may be that while the flux of methane between the ocean and atmosphere over the open oceans may have decreased or reversed sign, as suggested by *Cicerone and Oremland* [1988], the release from the continental shelf regions may not have changed substantially.

METHANE HYDRATES

Methane hydrates have recently become the subject of concern as a potentially large source of atmospheric methane [*Kvenvolden,* 1988; *Cicerone and Oremland,* 1988]. Recent releases of methane from methane hydrate destabilization are currently estimated by *Cicerone and Oremland* [1988] to be small, at around 5×10^{12} g CH_4 yr, however, this figure is very uncertain. In the future this release of methane could reach 100×10^{12} g CH_4 yr [*Kvenvolden,* 1988].

As we have only limited information on the extent, spatial and temporal variation in methane emission rates and cannot determine the total annual global release of methane from methane hydrates, a model for this methane emission was not included as a source in the atmospheric tracer transport model. However, as better information regarding the release of methane from methane hydrates becomes available this source of atmospheric methane will be included in the model.

MODEL SIMULATIONS WITH METHANE

All simulations with methane used the spatial and temporal distributions of the hydroxyl radical concentrations derived from the model of *Brasseur et al.* [1990]. The mean hydroxyl concentration, 6.37×10^5 molecules cm^{-3}, was that obtained from the methyl chloroform modeling studies, as reported earlier. The hydroxyl radical concentration specifies the most important loss term for atmospheric methane. Using this specified loss term for atmospheric methane along with a fixed loss of methane to the stratosphere, the total source of methane required to reproduce the observed atmospheric amounts and growth rate in atmospheric concentration can be derived. The total source of methane can be computed for any specified methane spatial and temporal source distributions.

Model initialization was achieved by specifying a latitudinal and vertical distribution of methane based upon the two-dimensional model results of *Brasseur et al.* [1990] for the month of January. The three-dimensional Lagrangian tracer transport model with methane sources and sinks was then integrated for 1 year. A second year of model integration generated the model results reported here.

The two methane source functions used in this study are summarized in Table 11. For source function 1 (SF1) the NPP-based approach, a total annual release of methane to the atmosphere of ~623 × 10^{12} g CH_4 was required to explain the observed growth in atmospheric methane concentration. Whereas, for source function 2 (SF2) a total annual release of methane to the atmosphere of ~ 611 × 10^{12} g CH_4 was needed to reproduce the observed growth in atmospheric methane concentration. These two estimates of the total source of methane are in excellent agreement. However, the predicted spatial and seasonal variation in the atmospheric methane concentrations differ. We shall consider each source function in turn.

Figure 19 shows the change in the globally averaged model surface layer (75 hPa) methane concentration. The methane concentration rises in the northern hemisphere summer and falls in the northern hemisphere winter. This seasonal cycle can be attributed to the high methane emission rates during the summer months in the northern hemisphere and larger loss in the southern hemisphere summer (as for CH_3CCl_3). The predicted amplitude of the seasonal cycle of methane, as illustrated in Figure 19, is larger than that observed at existing monitoring locations in the northern hemisphere [*Steele et al.*, 1987; *Blake and Rowland*, 1988]. However, methane observations only include measurements of marine boundary layer air masses. The larger amplitude of the model predicted methane seasonal cycle may be explained by the large seasonal cycle of atmospheric methane concentration over the source regions which is included in the model estimates of the seasonal cycle but which is not represented in the available observational data sets.

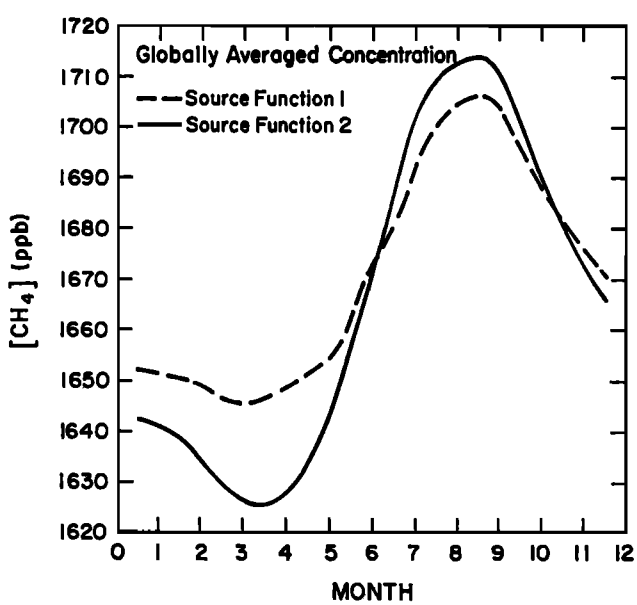

Fig. 19. Variation of the globally averaged model surface layer methane concentration with time based on source functions 1 and 2.

Figure 20 shows the seasonal cycles averaged over the model surface layer (75 hPa), for the northern and southern hemispheres and over oceanic regions of the respective hemispheres. The hemispheric averages include both the source regions and the tropics, whereas the oceanic averages are computed using the model grid squares over the Pacific ocean at mid-latitudes. These plots of the predicted methane concentration over the oceans show the importance of the sink of atmospheric methane and the seasonality of that sink.

Figure 21 shows a contour plot of the predicted methane concentrations over the model surface layer (75 hPa) for both January and July. As SF1 is largely based on a model of NPP a strong seasonality is evident in model predictions. This seasonality is particularly evident in the northern hemisphere. In January, only methane from fossil fuel is being released in high northern latitudes. In July the biospheric sources of methane are predicted to dominate the releases of methane in the northern latitudes. Concentrations rise in high northern latitudes in summer due to the large release of methane even though loss to reaction with the hydroxyl radical is at a peak.

Figure 22 illustrates the two-dimensional, zonally averaged, contour plot of the model predicted methane concentrations for the months of January and July. A drop in methane concentration with altitude and a distinct latitudinal gradient are predicted. These results are in good qualitative agreement with the latitudinal and vertical cross sections of methane concentration reported by *Marenco* [1988]. In particular, the model predicted elevated concentrations over northern latitude source regions and the tropics, the latitudinal gradient and the vertical gradient in methane concentration, were observed by *Marenco* [1988].

Figure 23 shows the predicted annual average methane concentrations corresponding to the National Oceanic and Atmospheric Administration Geophysical Monitoring for Climatic Change (NOAA/GMCC) sites along with the annual average methane concentrations calculated for 1984 from the monthly mean and spline fit data reported by *Steele et al.* [1987]. Estimated uncertainties in the annual average concentrations are based on the weighting parameter derived by *Steele et al.* [1987] which was considered an approximate measure of the average standard deviation of the data from the spline fit. Model predictions are in good agreement with the observed concentrations. However, it should be noted that the reported concentration data represent selected instantaneous point flask samples. It should also be noted that Figure 23 embodies the full three-dimensional nature of the atmospheric tracer transport model as the predicted concentrations were obtained from the individual grid cell corresponding to the latitude, longitude and altitude of the respective NOAA/GMCC sites.

Figure 24 shows the full zonal and annual averaged latitudinal distribution of methane concentration predicted for the model surface layer. The primary difference between Figure 24 and Figure 23, which presents the latitudinal gradient obtained at NOAA/GMCC sites, is the inclusion of the source regions which exhibit much

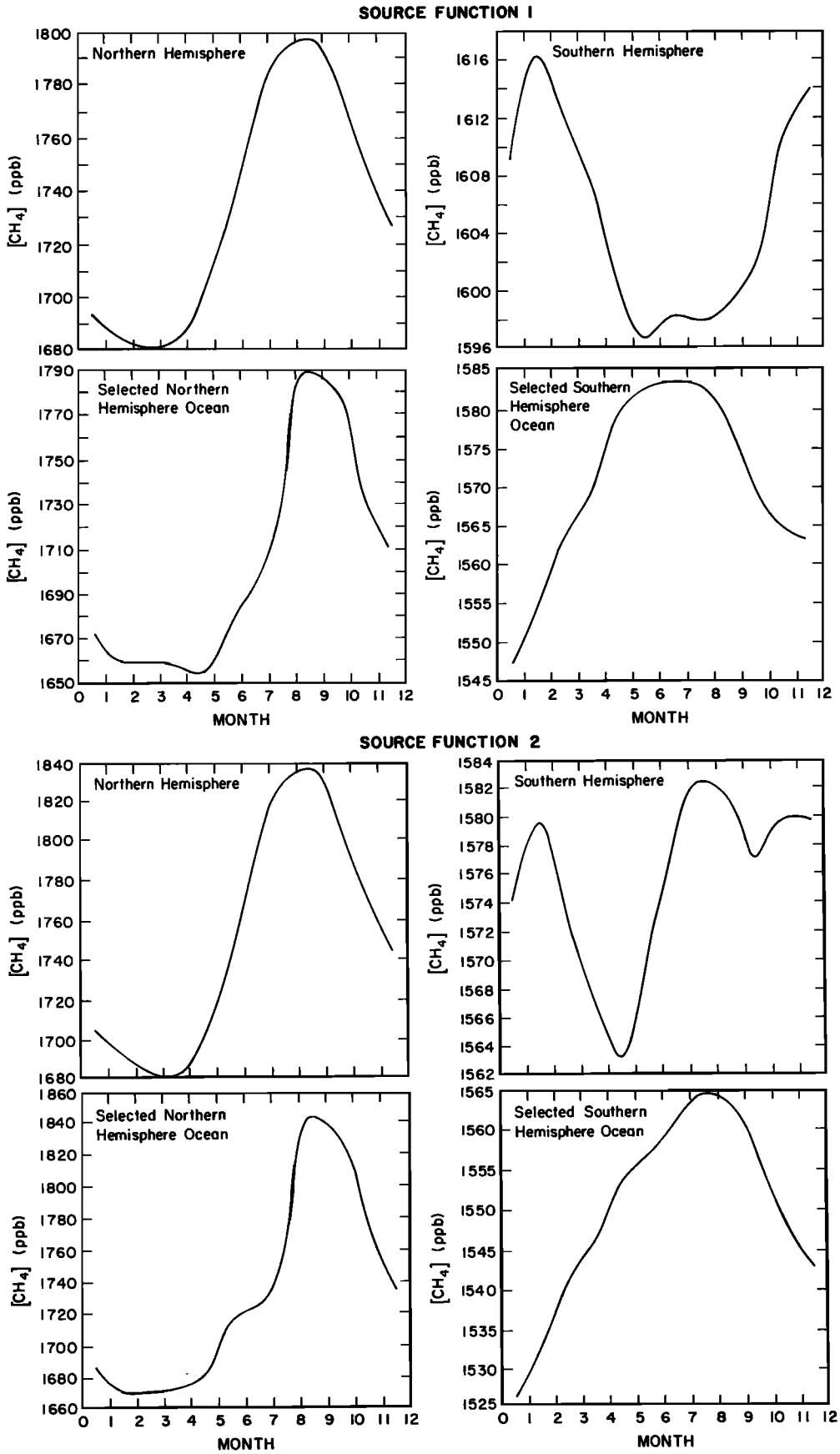

Fig. 20. Seasonal cycles of methane concentrations averaged over the northern and southern hemispheres and over oceanic regions of the respective hemispheres based on source functions 1 and 2.

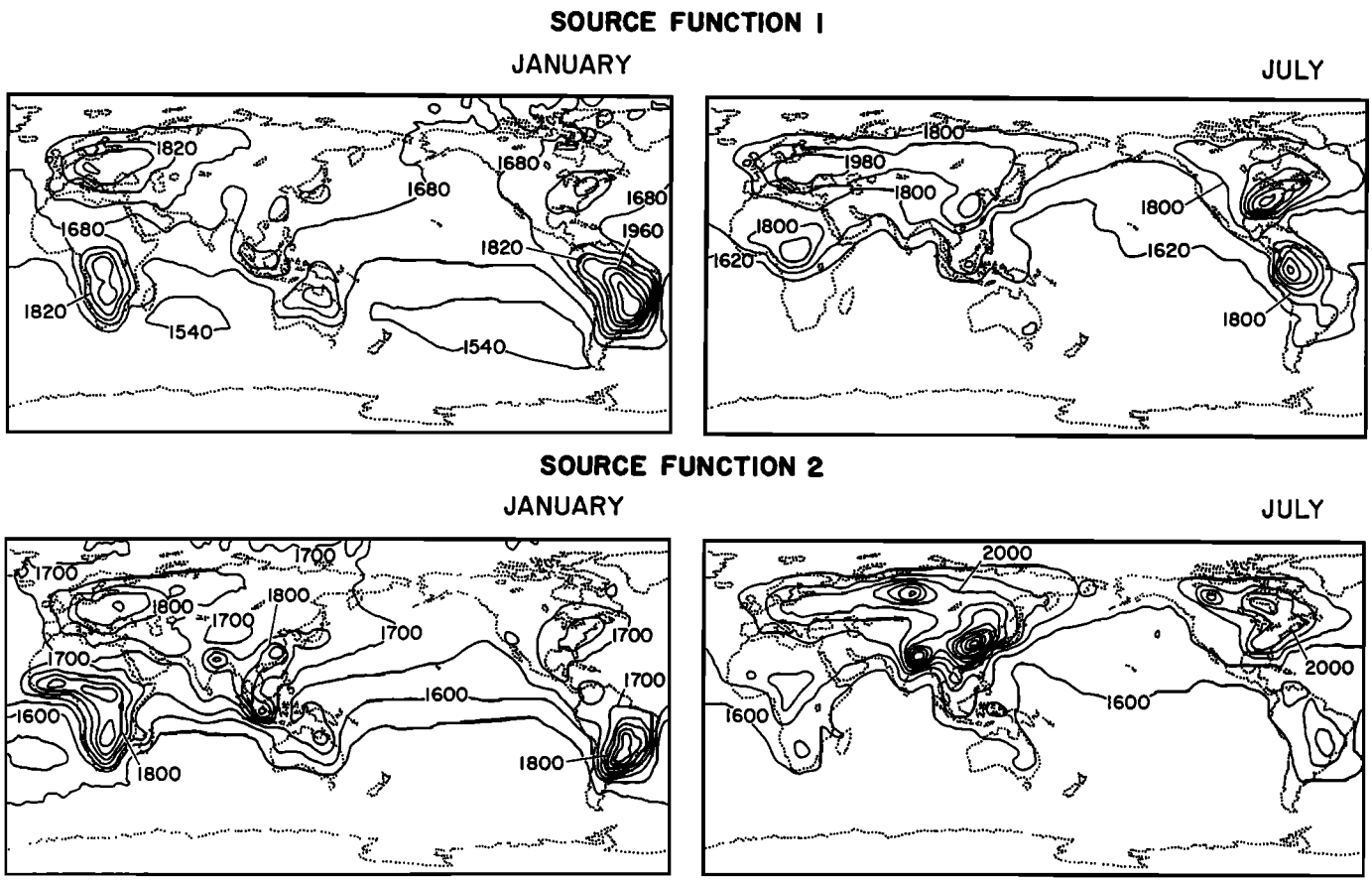

Fig. 21. Contour plot of the predicted methane concentrations (ppb) over the model surface layer for the months January and July based on source functions 1 and 2.

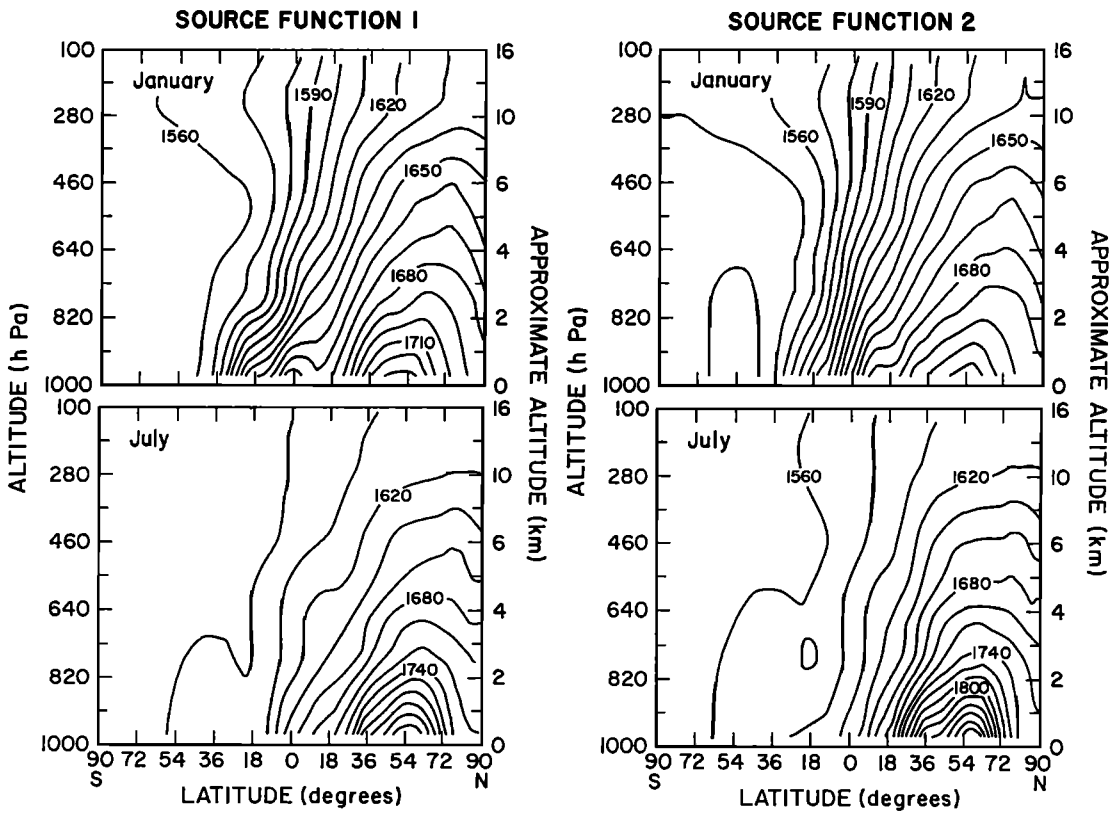

Fig. 22. Zonally averaged contour plots of the predicted methane concentrations (ppb) for the months of January and July based on source functions 1 and 2.

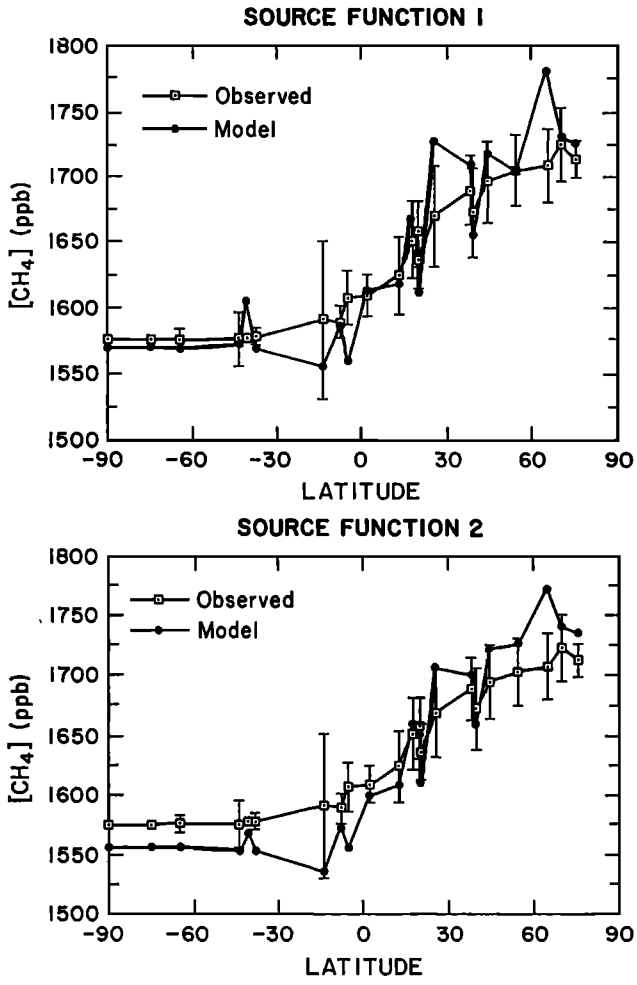

Fig. 23. The model predicted annual average methane concentrations, based on source functions 1 and 2, corresponding to the NOAA/GMCC sites along with the annual average methane concentrations for 1984 calculated from the monthly mean and spline fit data reported by *Steele et al.* [1987].

higher concentrations than observed at the NOAA/GMCC sites.

Figure 25 presents model predictions of monthly mean methane concentrations along with the observed concentrations, as reported by *Steele et al.* [1987], at four northern hemisphere and four southern hemisphere NOAA/GMCC sites. Model predictions and observations agree well at the southern hemisphere sites where the seasonal variation in atmospheric methane concentration is dominated by reaction with the hydroxyl radical. At Mauna Loa, in the northern hemisphere, the seasonal cycle is again correctly predicted. As Mauna Loa is located at some distance from the continental sources of atmospheric methane, the seasonal cycle is dominated by reaction with hydroxyl radical. The assumption of a lack of seasonality in methane emissions from the oceans would appear warranted based on the absence of a large difference between observations and model predictions of the seasonal cycle at Mauna Loa; however, this seasonal cycle could be too small to detect due to the low total release of methane from this source.

At midnorthern to high northern latitudes a significant difference between model predictions and observations has occurred. This disagreement may be the result of an improper model seasonal cycle of sources and/or sinks at these latitudes. The model predicts a maximum in the release of methane corresponding to the summer maximum in NPP. This maximum in concentration may be attributed to either too great a methane emission or too small a loss of methane to reaction with the hydroxyl radical. Figure 26 shows the predicted methyl chloroform concentrations along with the observed concentrations,

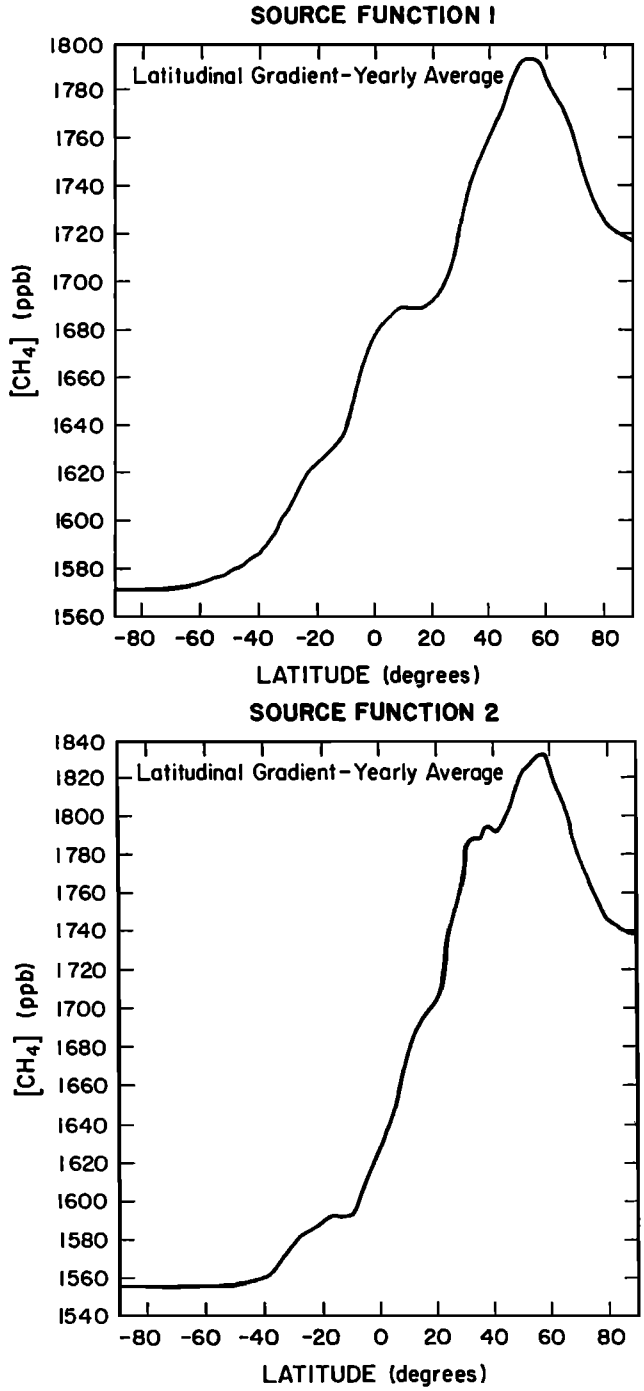

Fig. 24. The zonal and annual averaged latitudinal distribution of methane concentration predicted for the model surface layer based on source functions 1 and 2.

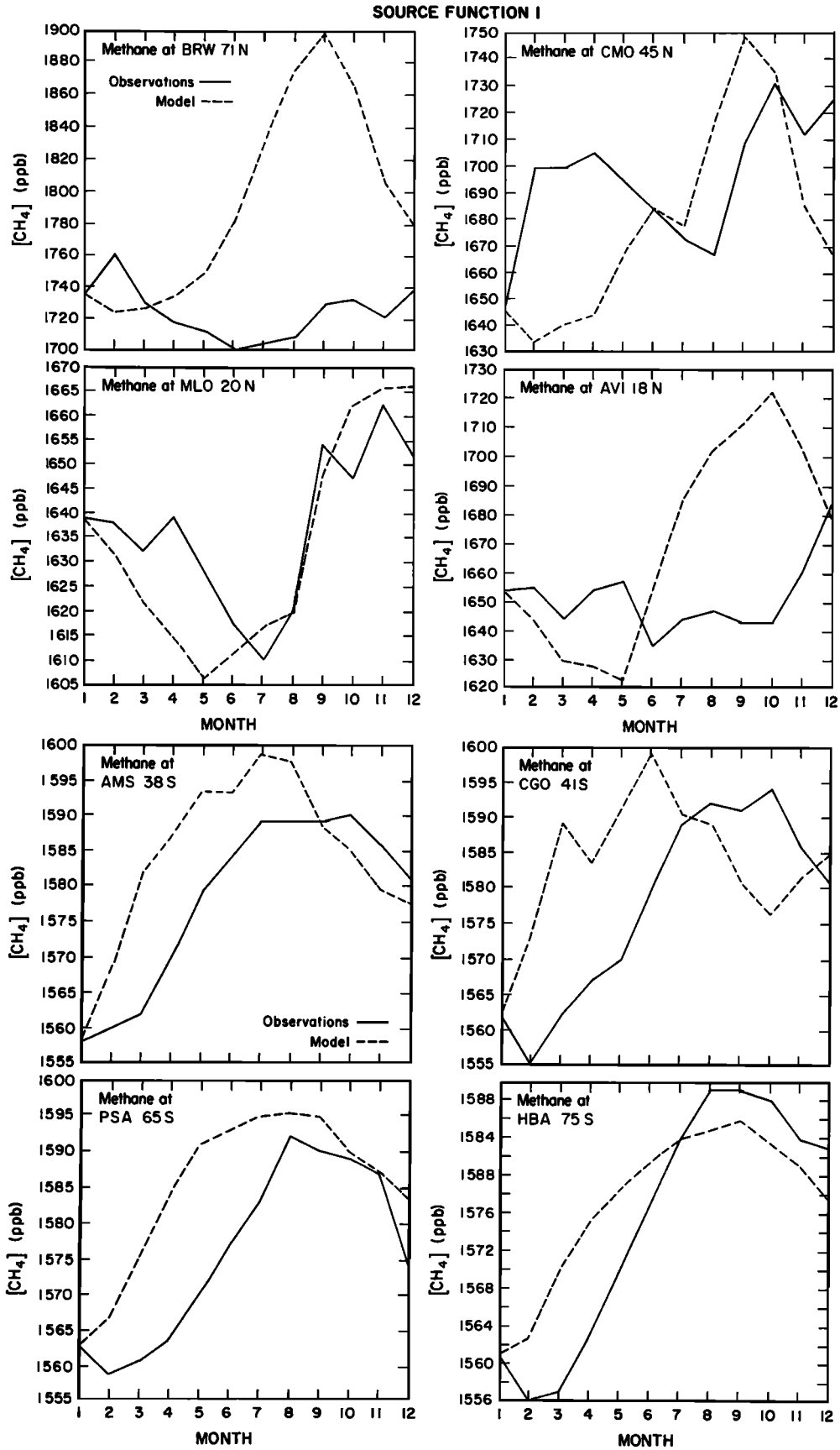

Fig. 25. Model predictions of monthly mean methane concentrations based on source functions 1 and 2 along with observed concentrations, as reported by *Steele et al.* [1987] at four northern and four southern hemisphere NOAA/GMCC sites. The model predictions have been adjusted to remove differences in scale by normalizing to the observed January concentration.

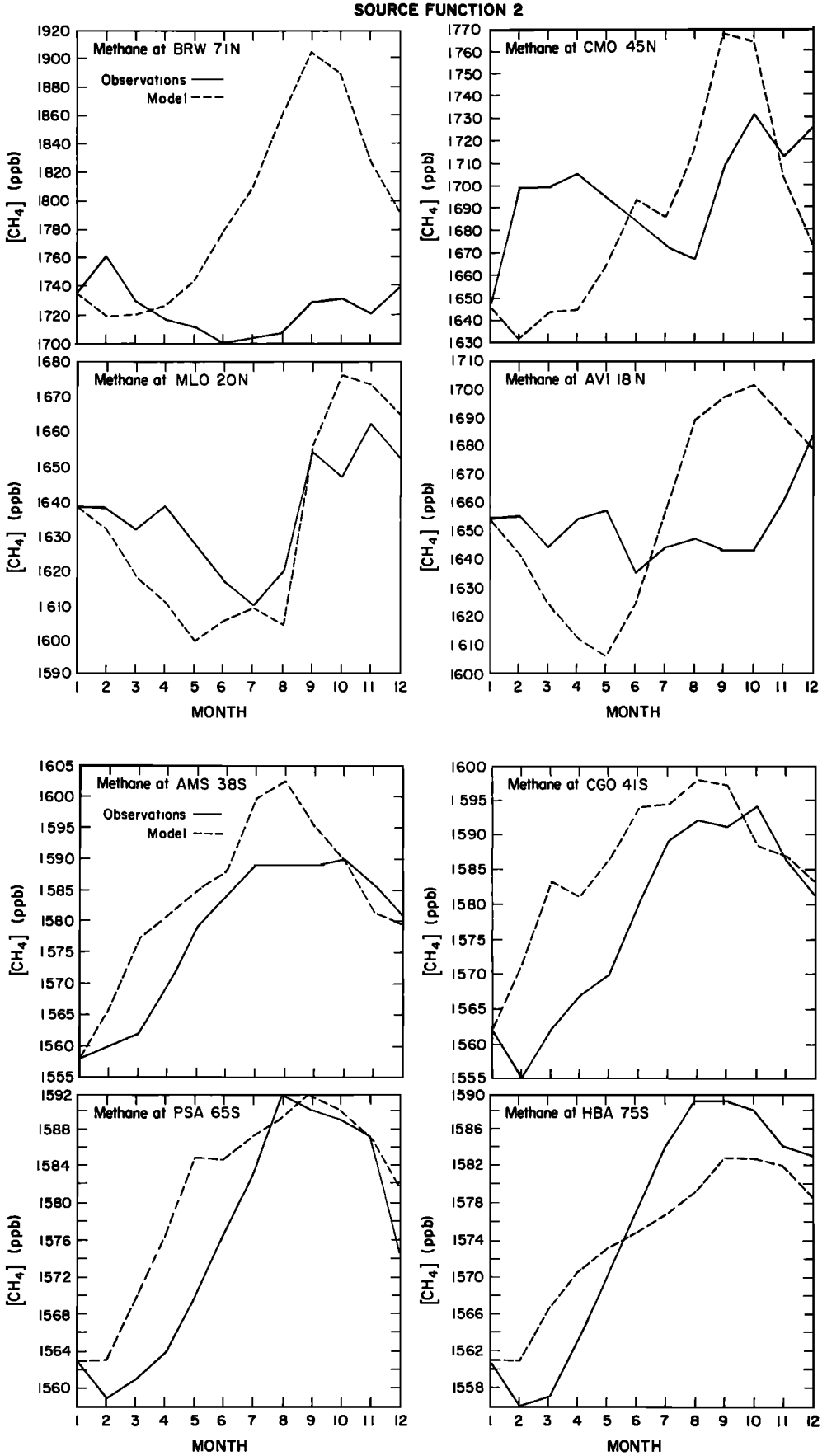

Fig. 25. (continued)

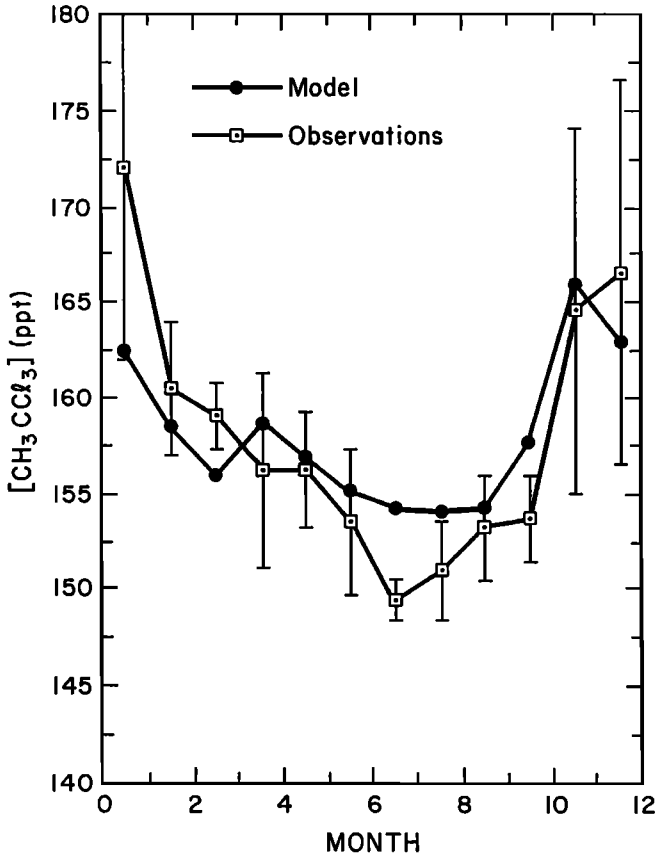

Fig. 26. Model predicted methyl chloroform concentrations along with the observed concentrations reported by *Khahil and Rasmussen* [1983] at Barrow, Alaska.

as reported by *Khalil and Rasmussen* [1983] at Barrow, Alaska. The model correctly predicts the drop in methyl chloroform concentration as a result of the increase in hydroxyl radical concentration during summer. As a consequence then, it would appear that the sources of methane at high northern latitudes are overpredicted during the summer. If the methane release was modeled to occur steadily throughout the year or during late autumn model predictions would more closely coincide with observations. An alternative explanation is that data selection may have lead to the systematic difference between observations and model predictions. For example, if concentrations in air masses which have traveled over the oceans were measured while air masses including continental air were discarded or not measured, then an actual increase in methane concentrations during summer would not be observed. This situation would arise as air arriving from over the oceans would be subjected to reaction with the high summer hydroxyl concentrations in the absence of sources of methane.

A similar set of model results are presented for SF2 as for SF1. Figure 19 also presents the change in the model surface layer (75 hPa), globally averaged, methane concentration with time. Figure 20 also shows for SF2 the predicted seasonal cycles of methane concentrations averaged over the model surface layer, for the northern and southern hemispheres and over oceanic regions of the hemispheres only. These results are very similar to those obtained for SF1.

Figure 21 also illustrates the variation in model predicted concentrations over the model surface layer (75 hPa) for both January and July for SF2. The major differences between SF1 and SF2 are apparent in these plots. A lower seasonal variation is predicted for SF2 in the high northern latitudes. However, the most striking difference lies in the methane concentrations eredicted over Southeast Asia. Here SF2, which includes a separate emission function for rice paddies, predicts much higher methane concentrations than SF1. Clearly, the assumption that a uniform fraction of NPP is converted to methane is not valid where rice paddies occur or NPP is grossly underestimated in these areas using the NPP model based on the Miami model of *Lieth* [1973, 1975] or the assumed methane releases from rice paddies (Table 5) are too large.

Figure 22 also illustrates the two-dimensional, zonally averaged, contour plot of the model predicted methane concentrations for SF2. Figure 22 shows that the model predicted vertical gradient is reversed over the southern hemisphere, where methane concentrations decrease with altitude, when compared with the northern hemisphere gradient during the month of January. During the month of July the vertical profile of methane concentration over the southern hemisphere is predicted to be more nearly constant. A similar result has been obtained for methyl chloroform as illustrated in Figure 10 and for SF1, as indicated in Figure 22. *Fraser et al.* [1986] have observed such changes in the vertical profile of methane over Cape Grim, Australia.

Figure 22 also indicates that SF2 produces smaller concentration gradients over the tropics and larger gradients over midnorthern latitudes than SF1. This result is in keeping with the greater magnitude of methane emissions from mid-northern latitudes by SF2. The lack of a significant vertical gradient over the equatorial regions, a result which is inconsistent with the observations of *Marenco* [1988], indicates that SF2 may be underpredicting methane emissions in the tropics. If this is the case then the source functions for termites, biomass burning, and/or wetlands include methane releases which are too low in the tropics.

Figure 23 also presents the predicted annual average methane concentration using SF2 corresponding to the NOAA/GMCC sites along with the annual average methane concentration calculated for 1984 from the monthly mean and spline fit data reported by *Steele* et al. [1987]. Again, estimated uncertainties in the annual average methane concentrations at each NOAA/GMCC site are based on the weighting parameter of *Steele* et al. [1987]. Figure 23 indicates that SF2 predicts higher northern latitude methane concentrations and lower southern hemisphere and equatorial methane concentrations than are observed.

Figure 24 also presents the zonally and annually averaged latitudinal gradient predicted by the model using SF2. The latitudinal gradient predicted using SF2 is much larger than that predicted by SF1. SF2 predicts much higher concentrations at mid-northern latitudes and lower concentration over the tropics than SF1.

Figure 25 also shows the model predictions of monthly mean methane concentrations along with the observed concentrations, as reported by *Steele et al.* [1987], at four northern hemisphere and four southern hemisphere

NOAA/GMCC sites. In general, similar agreement between model predictions and observations was obtained using SF2 and SF1. At the northern latitude sites SF2 precludes a larger disagreement with observations than SF1. Again, overprediction of methane concentrations at northern hemisphere sites may have occurred.

DISCUSSION

The magnitude of the methane sources determined in this study are sensitive to the assumed sinks of atmospheric methane. The total mass of methane released to the atmosphere has been determined by balancing the loss of methane to reaction with the hydroxyl radical and the relatively small loss to the stratosphere so that the observed growth in tropospheric methane concentration is reproduced. Should other sinks of tropospheric methane be demonstrated to be significant (for example consumption by soils), then the total of all sources of atmospheric methane would need to be revised upward. This potential systematic error confounds assessment of the error associated with the total sources of atmospheric methane. However, it can be assumed that the total source estimates reported here are more likely to represent a lower bound than an upper bound, if the average hydroxyl radical concentration remains valid.

The magnitude of the sources of atmospheric methane is also closely tied to the average hydroxyl radical concentration. We have estimated this quantity by using the reported methyl chloroform emissions data and atmospheric concentration data. However, our analysis indicated that a single constant value for the hydroxyl radical concentration could not be found that would lead to a predicted tropospheric concentration consistent with the estimated sources and concentration measurements. This result implies either of two possibilities (1) that a larger drop in hydroxyl radical concentrations has occurred than model studies would predict [*Thompson and Cicerone,* 1986; *Isaksen and Hov,* 1987]; or more likely (2) that the recent methyl chloroform emissions data may need revision upward. The need to revise methyl chloroform emissions upward is based upon a constant hydroxyl radical concentration calibrated to earlier estimates of methyl chloroform emissions. If these data also require revision upward than a concomitant increase in hydroxyl radical concentrations and the total methane emissions will be required. After completion of this study we became aware of the upward revision of estimated emissions of methyl chloroform of *Midgley* (1990).

The importance of methyl chloroform emissions data and tropospheric concentration measurements for an independent determination of the average hydroxyl radical concentration warrants a greater effort to evaluate the total emissions of methyl chloroform and its spatial and temporal distribution more precisely. Clearly, the characterization of the emissions of other trace gases which are entirely anthropogenic in origin, and for which the major sink is reaction with hydroxyl radicals in the troposphere, would provide independent estimates of the average hydroxyl radical concentration.

The average hydroxyl radical concentration that is deduced using methyl chloroform data will also be sensitive to the spatial and temporal distribution of the sources of methyl chloroform. If the majority of the emissions of methyl chloroform coincide with the highest hydroxyl radical concentrations then a much lower average hydroxyl concentration will be required to produce the same growth in atmospheric concentration than if methyl chloroform emissions occurred where hydroxyl radical concentrations are at their lowest. Accordingly, as the hydroxyl radical concentration varies over several orders of magnitude with respect to latitude, altitude, and season, accurate calculation of the average hydroxyl radical concentration requires at least two-dimensional atmospheric tracer transport models which take into account these variations in methyl chloroform emissions and hydroxyl radical concentration.

The assumption that a constant fraction of NPP is released as methane to the atmosphere appears, from a comparison of model results with available atmospheric methane measurements, to provide a reasonable source function for describing the spatial and temporal distribution of methane. Only at high northern latitudes are the model predictions of the seasonal cycle of atmospheric methane concentration not in agreement with the observed methane concentrations. However, this result is also true for SF2.

This disagreement between model predictions and observations indicates that either the previously predicted sources of methane are too large at high northern latitudes during summer for SF1 and to a greater extent for SF2 or that the observations of methane are not representative of the actual seasonal cycle of methane because of the data selection required to estimate long-term trends. Measurements directed at determining the true seasonal cycle of atmospheric methane at high northern latitudes will be required to resolve this problem. If the methane source functions must be modified to reduce the high northern latitude sources with a concomitant increase in the release of methane in low latitudes, then the total methane source will need to be increased. This increase in the total methane release to the atmosphere is required to account for the increased loss of methane due to the higher hydroxyl radical concentrations at low latitudes so that the observed increase in atmospheric methane concentration is correctly predicted.

The two source functions also produce slightly different latitudinal gradients. It is this difference in the latitudinal distribution of methane sources in combination with latitudinal variations in hydroxyl radical concentration which produces the difference in the estimates of the total methane source required to explain the observed growth in methane concentration. While SF1 more closely matches the latitudinal variation in annual average methane concentrations observed at NOAA/GMCC sites, true zonally averaged concentration estimates would greatly assist in determining the correct latitudinal distribution of methane sources and sinks.

A comparison of the methane concentration estimates obtained from the two atmospheric methane source functions shows that the models produce very similar results except where rice paddies are concentrated. Here SF2 predicts much higher atmospheric methane concentrations. Measurements of atmospheric methane concentrations near or above the rice paddies of Asia will be required to determine which source function provides a realistic representation of the release of methane from rice paddies.

Unfortunately, only a limited number of tracer concentration measurements are presently available to validate tracer transport model predictions. Available measurements of atmospheric trace gas concentrations currently provide important information regarding the long term trends. However, the practice of reporting selected data makes the direct comparison of such observations with the output of atmospheric tracer transport models difficult. Monitoring sites are also located away from source regions making validation of model predicted concentrations over such regions very difficult. In order to more fully validate atmospheric tracer transport models a measurement program aimed at obtaining latitudinal and zonal profiles, both over the continents and oceans, is required. Measurements could consist of either point measurements at different altitudes or, tropospheric column averages, or vertical profiles. Measurement techniques which produce area or column averages rather than point values would be preferred, as transport model predictions represent large volume averages.

Finally, a recent measurement of the reaction rate of hydroxyl radical and methane by *Vaghjiani and Ravishankara* [1990] indicates that the rate is lower than previously measured. Using the rate coefficient of Ravishankara in the three-dimensional model, we calculated that the sources listed in Table 11 should be multiplied by a factor of 0.83 if the observed growth in atmospheric methane concentrations is to be reproduced. This would lead to an estimated atmospheric residence time of 10.0 and 10.2 years for methane for the respective source functions. The major difference in predicted methane concentrations will be a reduction in the amplitude of seasonal cycle of methane concentrations. This leads to improved model predictions of observations collected at most NOAA/GMCC monitoring sites. These results are provisional, pending any revision of the reaction rate for OH + $C_2H_3Cl_3$.

CONCLUSIONS

A global three-dimensional Lagrangian tracer transport model has been employed to study the sources and sinks of atmospheric methane. A global average tropospheric hydroxyl radical concentration of 6.4×10^5 cm^{-3} was determined using published methyl chloroform emissions and atmospheric concentration data. Southern hemisphere averaged OH was 7.2×10^5 cm^{-3} and northern hemisphere OH was 5.5×10^5 cm^{-3}. For the years 1981–1984, methyl chloroform emissions data were found to be inconsistent with the observed growth in atmospheric concentration if a constant or near-constant average hydroxyl radical concentration is assumed. The hydroxyl radical concentration must fall $\sim$ 25% to produce the observed growth in methyl chloroform concentration over the period 1981–1984. The more likely situation is that the methyl chloroform emissions for 1981–1984 need upward revision.

Two source functions describing the spatial and temporal distribution of the flux of methane to the atmosphere were developed. The first model, SF1, assumed that the releases of methane from rice paddies, wetlands, enteric fermentation, termites, and biomass burning were proportional to net primary productivity. Model-predicted methane concentrations were in good agreement with available observations except at high northern latitude NOAA/GMCC sites. Including releases of methane from fossil fuels, landfills and the oceans an annual source of $\sim$ 623 Tg CH_4 was required to explain the observed growth in atmospheric methane concentration. A globally averaged atmospheric lifetime of 8.3 years is deduced from SF1. With a new, slower rate constant for OH plus methane, this lifetime is raised to 10.0 years.

The second source function, SF2, separately identified the releases of methane from rice paddies, wetlands, enteric fermentation, termites and biomass burning. The major difference between SF1 and SF2 is the prediction of an intense release of methane corresponding to the rice paddies of Asia and Southeast Asia by SF2. SF2 leads to a different latitudinal distribution of the release of methane with a greater release of methane occurring at higher latitudes than SF1. Accordingly, SF2 leads to a lower estimate of the total methane source of $\sim$ 611 Tg. A globally averaged atmospheric lifetime of 8.5 years is deduced from SF2. With a new, slower rate constant for OH plus methane, this lifetime becomes 10.2 years. SF2 also produces estimates of atmospheric methane concentration which are in poorer agreement with NOAA/GMCC observations of methane at high northern latitudes than SF1.

On the basis of the model, results obtained using both methane source functions developed in this study it would appear that further investigation of the sources and sinks of methane at high northern latitudes is warranted. Measurements of atmospheric methane with the objective of determining methane sources and sinks rather than just long-term trends are also required.

Acknowledgments. The authors would like to thank Phillip Rasch, David Lowe, Stanley Tyler, Robert Chatfield, and the referees for useful discussions and comments on earlier drafts. We would also like to thank Michael Prather for providing his F-11 source distribution and ECMWF for providing the wind fields. One of us, J.A.T., acknowledges the support of the National Oceanic and Atmospheric Administration Geophysical Monitoring for Climatic Change program for support. R.J.C. acknowledges support from NASA contract W-16,184. The National Center for Atmospheric Research is sponsored by the National Science Foundation.

REFERENCES

Allam, R. J., K. S. Groves, and A. F. Tuck, Global OH distribution derived from general circulation model fields of ozone and water vapor, *J. Geophys. Res., 86,* 5303–5320, 1981.

Anderson, J. G., W. H. Brune, and M. H. Proffitt, Ozone destruction by chlorine radicals within the Antarctic vortex: The spatial and temporal evolution of ClO-O_3 anticorrelation based on in situ ER-2 data, *J. Geophys. Res., 94,* 11,465–11,479, 1989.

Aselmann, I., and P. J. Crutzen, Global distribution of natural freshwater wetlands and rice paddies, their net primary productivity, seasonality and possible methane emissions, *J. Atmos. Chem., 8,* 307–358, 1989.

Bingemer, H. G., and P. J. Crutzen, The production of methane from solid wastes, *J. Geophys. Res., 92,* 2181–2187, 1987.

Blake, D. R., and F. S. Rowland, Continuing worldwide increase in tropospheric methane, 1978 to 1987, *Science, 239,* 1129–1131, 1988.

Box, E., Quantitative evaluation of global primary productivity models generated by computers, in *Primary Productivity of the Biosphere,* edited by H. Lieth and R. H. Whittaker, pp. 265–283, Springer-Verlag, New York, 1975.

Brasseur, G., M. H. Hitchman, S. Walters, M. Dymek, E. Falise, and M. Pirre, An interactive chemical dynamical radiative two-dimensional model of the middle atmosphere, *J. Geophys. Res., 95,* 5639–5655, 1990.

Chameides, W. L., and A. Tan, The two-dimensional diagnostic model for tropospheric OH: An uncertainty analysis, *J. Geophys. Res., 86,* 5209–5223, 1981.

Cicerone, R. J., and R. S. Oremland, Biogeochemical aspects of atmospheric methane, *Global Biogeochem. Cycles, 2,* 299–327, 1988.

Cicerone, R. J., and J. D. Shetter, Sources of atmospheric methane: Measurements in rice paddies and a discussion, *J. Geophys. Res., 86,* 7203–7209, 1981.

Cicerone, R. J., J. D. Shetter, and C. C. Delwiche, Seasonal variation of methane flux from a California rice paddy, *J. Geophys. Res., 88,* 11,022–11,024, 1983.

Cogley, J. G., THYDRO: A terrestrial hydrographic data set, *Tech. Note 85-4,* Trent University, Peterborough, Ontario, Canada, 1985.

Collins, N. M., and T. G. Wood, Termites and atmospheric gas production, *Science, 224,* 84–86, 1984.

Craig, H., and C. C. Chou, Methane: The record in polar ice cores, *Geophys. Res. Lett., 9,* 1221–1224, 1982.

Crill, P. M., K. B. Bartlett, R. C. Harriss, E. Gorham, E. S. Verry, D. I. Sebacher, L. Madzar, and W. Sanner, Methane flux from Minnesota peatlands, *Global Biogeochem. Cycles, 2,* 371–384, 1988.

Crutzen, P. J., Role of the tropics in atmospheric chemistry, in *The Geophysiology of Amazonia,* edited by R. E. Dickinson, pp. 107–130, John Wiley, New York, 1987.

Crutzen, P. J., and J. Fishman, Average concentrations of OH in the troposphere, and the budgets of CH_4, CO, H_2 and CH_3CCl_3, *Geophys. Res. Lett., 4,* 321–324, 1977.

Crutzen, P. J., and L. T. Gidel, A two-dimensional photochemical model of the atmosphere, 2, The tropospheric budgets of the anthropogenic chlorocarbons CO, CH_4, CH_3Cl, and the effect of various NO_x sources on tropospheric ozone, *J. Geophys. Res., 88,* 6641–6661, 1983.

Crutzen, P. J., L. E. Heidt, J. P. Krasnec, W. H. Pollock, and W. Seiler, Biomass burning as a source of atmospheric gases CO, H_2, N_2O, NO, CH_3Cl and COS, *Nature, 282,* 253–256, 1979.

Crutzen, P. J., A. C. Delany, J. Greenberg, P. Haagenson, L. Heidt, R. Lueb, W. Pollock, W. Seiler, A. Wartburg, and P. Zimmerman, Tropospheric chemical composition measurements in Brazil during the dry season, *J. Atmos. Chem., 2,* 233–256, 1985.

Crutzen, P. J., I. Aselmann, and W. Seiler, Methane production by domestic animals, wild ruminants, other herbivorous fauna, and humans, *Tellus, 38B,* 271–284, 1986.

Cunnold, D. M., R. G. Prinn, R. A. Rasmussen, P. G. Simmonds, F. N. Alyea, C. A. Cardelino, A. J. Crawford, P. J. Fraser, and R. D. Rosen, The atmospheric lifetime experiment, 3, Lifetime methodology and applications to three years of $CFCl_3$ data, *J. Geophys. Res., 88,* 8379–8400, 1983*a*.

Cunnold, D. M., R. G. Prinn, R. A. Rasmussen, P. G. Simmonds, F. N. Alyea, C. A. Cardelino, and A. J. Crawford, The atmospheric lifetime experiment, 4, Results for CF_2Cl_2 based on three years data, *J. Geophys. Res., 88,* 8401–8414, 1983*b*.

Davis, D. D., W. Heaps, and T. McGee, Direct measurements of natural tropospheric levels of OH via an aircraft borne tunable bye laser, *Geophys. Res. Lett., 3,* 331–333, 1976.

Delany, A. C., P. Haagensen, S. Walters, and A. F. Wartburg, Photochemically produced ozone in the emission from large-scale tropical vegetation fires, *J. Geophys. Res., 90,* 2425–2429, 1985.

Derwent, R. G., and A. E. J. Eggleton, Two-dimensional model studies of methyl chloroform in the troposphere, *Quart. J. R. Meteorol. Soc., 107,* 231–242, 1981.

Dickinson, R. E., and R. J. Cicerone, Future global warming from atmospheric trace gases, *Nature, 319,* 109–115, 1986.

Ehhalt, D. H., The atmospheric cycle of methane, *Tellus, 26,* 58–70, 1974.

Ehhalt, D. H., and L. E. Heidt, Vertical profiles of CH_4 in the troposphere and stratosphere, *J. Geophys. Res., 78,* 5265–5272, 1973.

Ehhalt, D. H., and U. Schmidt, Sources and sinks of atmospheric methane, *Pure Appl. Geophys., 116,* 452–464, 1978.

Fishman, J., Tropospheric ozone from satellite total ozone measurements, in *Tropospheric Ozone,* edited by I. S. A. Isaksen, pp. 111–123, D. Reidel, Hingham, Mass., 1988.

Fishman, J., P. Minnis, and H. G. Reichle, Jr., Use of satellite data to study tropospheric ozone in the tropics, *J. Geophys. Res., 91,* 14,451–14,465, 1986.

Fraser, P. J., P. Hyson, R. A. Rasmussen, A. J. Crawford, and M. A. K. Khalil, Methane, carbon monoxide and methyl chloroform in the southern hemisphere, *J. Atmos. Chem., 4,* 3–42, 1986.

Golombek, A., and R. G. Prinn, A global three-dimensional model of the circulation and chemistry of $CFCl_3$, CF_2Cl_2, CH_3CCl_3, CCl_4, and N_2O, *J. Geophys. Res., 91,* 3985–4001, 1986.

Greenberg, J. P., P. R. Zimmerman, and R. B. Chatfield, Hydrocarbons and carbon monoxide in African savannah air, *Geophys. Res. Lett., 12,* 113–116, 1985.

Harriss, R. C., D. I. Sebacher, and F. P. Day, Methane flux in the great dismal swamp, *Nature, 297,* 673–674, 1982.

Henderson-Sellers, A., M. F. Wilson, G. Thomas, and R. E. Dickinson, Current global land-surface data sets for use in *NCAR/TN-272+STR,* Natl. Cent. for Atmos. Res., Boulder, Colo., 1986.

Holzapfel-Pschorn, A., and W. Seiler, Methane emission during a cultivation period from an Italian rice paddy, *J. Geophys. Res., 91,* 11,803–11,814, 1986.

Hsu, C. F., Air parcel motions during a numerically simulated stratospheric warming, *J. Atmos. Sci., 37,* 2768-2792, 1980.

Hübler, G., D. Perner, U. Platt, A. Tönnissen, and D. H. Ehhalt, Ground level OH radical concentration: New measurements by optical absorption, *J. Geophys. Res., 89,* 1309–1319, 1984.

Hungate, R. E., *The Rumen and Its Microbes,* 533 pp., Academic, San Diego, Calif., 1966.

Isaksen, I. S. A., and O. Hov, Calculation of trends in the tropospheric concentration of O_3, OH, CH_4 and NO_x, *Tellus, 39B,* 271–285, 1987.

Jacob, D. J., M. J. Prather, S. C. Wofsy, and M. B. McElroy, Atmospheric distribution of ^{85}Kr simulated with a general circulation model, *J. Geophys. Res., 92,* 6614–6626, 1987.

Justus, C. G., *Winds and Wind System Performance,* The Franklin Institute Press, Philadelphia, Pa., 1978.

Khalil, M. A. K., and R. A. Rasmussen, Gaseous tracers of Arctic haze, *Environ. Sci. Technol., 17,* 157–164, 1983.

Koyama, T., Gaseous metabolism in lake sediments and paddy soils and the production of atmospheric methane and hydrogen, *J. Geophys. Res., 68,* 3971–3973, 1963.

Kvenvolden, K., Methane hydrates and global climate, *Global Biogeochem. Cycles, 2,* 221–229, 1988.

Lieth, H., Primary production: Terrestrial ecosystems, *Human Ecol., 1,* 303–332, 1973.

Lieth, H., Modeling the primary productivity of the world, in *Primary Productivity of the Biosphere,* edited by H. Lieth and R. H. Whittaker, pp. 237–263, Springer-Verlag, New York, 1975.

Lerner, J., E. Matthews, and I. Fung, Methane emission from animals: A global high-resolution data base, *Global Biogeochem. Cycles, 2,* 139–156, 1988.

Logan, J. A., and V. W. J. H. Kirchhoff, Seasonal variations of tropospheric ozone at Natal, Brazil, *J. Geophys. Res., 91,* 7875–7881, 1986.

Lorenc, A. C., A global three-dimensional multivariate statistical interpolation scheme, *Mon. Weather Rev., 109,* 701–721, 1981.

Lovelock, J. E., Methyl chloroform in the troposphere as an indicator of OH radical abundance, *Nature, 267,* 32, 1977.

Lowe, D. C., C. A. M Brenninkmeijer, M. R. Manning, R. Sparks, and G. Wallace, Radiocarbon determination of atmospheric methane at Baring Head, New Zealand, *Nature, 332,* 522–525, 1988.

Marenco, A., Large scale distributions of O_3, CO and CH_4 in the troposphere from scientific aircraft measurements (STRATOZ III), in *Tropospheric Ozone,* edited by I. S. A. Isaksen, pp. 73–81, D. Reidel, Hingham, Mass., 1988.

Marland, G., R. M. Rotty, and N. L. Treat, CO_2 from fossil fuel burning: Global distribution of emissions, *Tellus, 37B,* 243–258, 1985.

Matthews, E., and I. Fung, Methane emission from natural wetlands: Global distribution, area, and environmental characteristics of sources, *Global Biogeochem. Cycles, 1,* 61–86, 1987.

Midgley, P. M., The production and release to the atmosphere of 1,1,1-trichloroethane (methylchloroform), *Atmos. Environ.,* 2663–2665, 1989.

Neely, W. B., and J. H. Plonka, Estimation of time-averaged hydroxyl radical concentration in the troposphere, *Environ. Sci. Technol., 12,* 317–321, 1978.

Olson, J. S., J. A. Watts, and L. J. Allison, Carbon in live vegetation of major world ecosystems, *Dep. of Energy Rep. DOE/NBB-0037,* 191 pp., Oak Ridge Natl. Lab., Oak Ridge, Tenn., 1983.

Oort, A., Global atmospheric circulation statistics, 1958–1973, *Prof. Pap. 14,* Natl. Oceanic and Atmos. Admin., Boulder, Colo., 1983.

Pearman, G. I., and P. J. Fraser, Sources of increased atmospheric methane, *Nature, 332,* 489–490, 1988.

Perner, D., U. Platt, M. Trainer, G. Hübler, J. Drummond, W. Junkermann, J. Rudolph, B. Schubert, A. Volz, D. H. Ehhalt, K. J. Rumpel, and G. Helas, Measurements of tropospheric OH concentrations: A comparison of field data with model predictions, *J. Atmos. Chem., 5,* 185–216, 1987.

Platt, U., M. Rateike, W. Junkermann, J. Rudolph, and D. H. Ehhalt, New tropospheric OH measurements, *J. Geophys. Res., 93,* 5159–5166, 1988.

Prather, M. J., Continental sources of halocarbons and nitrous oxide, *Nature, 317,* 221–225, 1985.

Prather, M., M. McElroy, S. Wofsy, G. Russel, and D. Rind, Chemistry of the global troposphere: Fluorocarbons as tracers of air motion, *J. Geophys. Res., 92,* 6579–6613, 1987.

Prinn, R. G., R. A. Rasmussen, P. G. Simmonds, F. N. Alyea, D. M. Cunnold, B. C. Lane, C. A. Cardelino, and A. J. Crawford, The atmospheric lifetime experiment, 5, Results for CH_3CCl_3 based on three years of data, *J. Geophys. Res., 88,* 8415–8426, 1983*a*.

Prinn, R. G., P. G. Simmonds, R. A. Rasmussen, R. D. Rosen, F. N. Alyea, C. A. Cardelino, A. J. Crawford, D. M. Cunnold, P. J. Fraser, and J. E. Lovelock, The atmospheric lifetime experiment, 1, Introduction, instrumentation, and overview, *J. Geophys. Res., 88,* 8353–8367, 1983*b*.

Prinn, R., D. Cunnold, R. Rasmussen, P. Simmonds, F. Alyea, A. Crawford, P. Fraser, and R. Rosen, Atmospheric trends in methyl chloroform and the global average for the hydroxyl radical, *Science, 238,* 945–950, 1987.

Ramanathan, V., L. Callis, R. Cess, J. Hansen, I. Isaksen, W. Kuhn, A. Lacis, F. Luther, J. Mahlman, R. Reck, and M. Schlesinger, Climate-chemical interactions and effects of changing atmospheric trace gases, *Rev. Geophys., 25,* 1441–1482, 1987.

Rasmussen, R. A., and M. A. K. Khalil, Latitudinal distributions of trace gases in and above the boundary layer, *Chemosphere, 11,* 227-235, 1982.

Rasmussen, R. A., and M. A. K. Khalil, Global production of methane by termites, *Nature, 301,* 700–702, 1983.

Rasmussen, R. A., and M. A. K. Khalil, Atmospheric methane in the recent and ancient atmospheres: Concentrations, trends, and interhemispheric gradient, *J. Geophys. Res., 89,* 11,599–11,605, 1984.

Rasmussen, R. A., M. A. K. Khalil, and J. S. Chang, Atmospheric trace gases over China, *Environ. Sci. Technol., 16,* 124–126, 1982.

Rotty, R. M., A look at 1983 CO_2 emissions from fossil fuels (with preliminary data for 1984), *Tellus, 39B,* 203–208, 1987*a*.

Rotty, R. M., Estimates of seasonal variation in fossil fuel CO_2 emissions, *Tellus, 39B,* 184–202, 1987*b*.

Seiler, W., Contribution of biological processes to the global budget of CH_4 in the atmosphere, in *Current Perspectives in Microbial Ecology,* edited by M. J. Klug and C. A. Reddy, pp. 468–477, American Society for Microbiology, Washington, D. C., 1984.

Seiler, W., and P. J. Crutzen, Estimates of gross and net fluxes of carbon between the biosphere and the atmosphere from biomass burning, in *Climatic Change,* Vol. 2, pp. 207–247, D. Reidel, Hingham, Mass., 1980.

Seiler, W., A. Holzapfel-Pschorn, and R. Conrad, Methane emission from rice paddies, *J. Atmos. Chem., 1,* 241–268, 1984.

Shea, D. J., Climatological Atlas: 1950–1979, *Tech. Note NCAR/TN-269+STR,* Natl. Cent. for Atmos. Res., Boulder, Colo., 1986.

Sheppard, J. C., H. Westberg, J. F. Hopper, K. Ganesan, and P. Zimmerman, Inventory of global methane sources and their production rates, *J. Geophys. Res., 87,* 1305–1312, 1982.

Singh, H. B., Atmospheric halocarbons: Evidence in favor of reduced average hydroxyl radical concentration in the troposphere, *Geophys. Res. Lett., 4,* 101–104, 1977.

Stauffer, B., G. Fischer, A. Neftel, and H. Oeschger, Increases in atmospheric methane recorded in Antarctic ice core, *Science, 229,* 1386–1388, 1985.

Steele, L. P., P. J. Fraser, R. A. Rasmussen, M. A. K. Khalil, T. J. Conway, A. J. Crawford, R. H. Gammon, K. A. Masarie, and K. W. Thoning, The global distribution of methane in the troposphere, *J. Atmos. Chem., 5,* 125–171, 1987.

Taylor, J. A., A stochastic Lagrangian atmospheric transport model to determine global CO_2 sources and sinks–a preliminary discussion, *Tellus, 41B,* 272–285, 1989.

Thompson, A. M., and R. J. Cicerone, Possible perturbations to atmospheric CO, CH_4, and OH, *J. Geophys. Res., 91,* 10,853–10,864, 1986.

Volz, A., D. H. Ehhalt, and R. G. Derwent, Seasonal and latitudinal variation of ^{14}CO and the tropospheric concentration of OH radicals, *J. Geophys. Res., 86,* 5163–5171, 1981.

Wahlen, M., N. Tanaka, R. Henry, B. Deck, J. Zeglen, J. S. Vogel, J. Southon, A. Shemesh, R. Fairbanks, and W. Broecker, Carbon-14 in methane sources and in atmospheric methane: The contribution from fossil carbon, *Science, 245,* 286–290, 1989.

Walton, J. J., M. C. MacCracken, and S. J. Ghan, A global-scale Lagrangian trace species model of transport, transformation, and removal processes, *J. Geophys. Res., 93,* 8339–8354, 1988.

Wang, C. C., L. I. Davis, Jr., C. H. Wu, S. Japar, H. Niki, and B. Weinstock, Hydroxyl radical concentrations measured in ambient air, *Science, 189,* 797–800, 1975.

Warneck, P., OH production rates in the troposphere, *Planet. Space Sci., 23,* 1507–1518, 1975.

Whalen, S. C., and W. S. Reeburgh, A methane flux time series for tundra environments, *Global Biogeochem. Cycles, 2,* 399–409, 1988.

Williamson D. L., and P. J. Rasch, Two-dimensional semi-Lagrangian transport with shape-preserving interpolation, *Mon. Weather Rev., 117,* 102-129, 1989.

Weinstock, B., and T. Y. Chang, The global balance of carbon monoxide, *Tellus, 26,* 108–115, 1974.

Wilson, M. F., and A. Henderson-Sellers, A global archive of land cover and soils data for use in general circulation climate models, *J. Climatol., 5,* 119–143, 1985.

Wofsy, S. C., Atmospheric CH_4, CO, and CO_2, *J. Geophys. Res., 77,* 4477–4493, 1972.

Wong, C. S., Atmospheric input of carbon dioxide from burning wood, *Science, 200,* 197–200, 1978.

Zimmerman, P. R., J. P. Greenberg, S. O. Wandiga, and P. J. Crutzen, Termites: A potentially large source of atmospheric methane, carbon dioxide and molecular hydrogen, *Science, 218,* 563–565, 1982.

Zimmerman, P. R., J. P. Greenberg, and J. P. E. C. Darlington, Response to "Termites and atmospheric gas production" (technical comment by N. M. Collins and T. G. Wood), *Science, 224,* 84–86, 1984.

G. Brasseur, R. Cicerone, and P. Zimmerman, National Center for Atmospheric Research, P. O. Box 3000, Boulder, CO 80307.

J. A. Taylor, Cooperative Institute for Research in the Environmental Sciences, University of Colorado, Boulder, CO 80309.

(Received January 2, 1990;
revised September 7, 1990;
accepted September 7, 1990.)